

1

1 The Neurophenomenology of a Self-Induced Transcendental Visionary
2 State: A Case Study

3

4 Gabriel Della Bella^{+a,b}, Agustina Velez Picatto^{+a}, Dante Sebastián Galván Rial^a,
5 Sebastián Cukier^c, Gustavo Foa Torres^d, Magaly Catanzariti^e, Diego Mateos^{e,f,g},
6 Pedro Lamberti^b, Etzel Cardeña^{h*}, Pablo Barttfeld^{a*}

7 a- Cognitive Science Group, Instituto de Investigaciones Psicológicas (IIPsi, CONICET-UNC),
8 Facultad de Psicología, Universidad Nacional de Córdoba, Córdoba, Argentina.

9 b- Facultad de Matemática, Astronomía, Física y Computación, Universidad Nacional de Córdoba,
10 Córdoba, Argentina.

11 c- Hospital Elizalde, Casa Cuna, Buenos Aires, Argentina.

12 d- Instituto Oulton, Córdoba, Argentina.

13 e- Instituto de Matemática aplicada del Litoral (IMAL-CONICET-UNL), Santa Fe, Argentina.

14 f- Universidad Autónoma de Entre Ríos (UADER), Entre Ríos, Argentina.

15 g- Achucarro Basque Center for Neuroscience, Leioa (Bizkaia), Spain.

16 h- Center for Research on Consciousness and Anomalous Psychology (CERCAP), Department of
17 Psychology, Lund University, Lund, Sweden.

18

19 + First author

20 * Last author

21 Corresponding author: Gabriel Della Bella dellabellagabriel@gmail.com

22

23

24

25

26

27

28

29

30

31

32

33

34

35

36 Abstract

37 Non-ordinary states of consciousness (NOC) offer a way to examine how large-scale brain
38 dynamics reorganize as experience changes. We studied a participant able to reliably enter
39 a self-induced NOC state characterized by vivid imagery, altered bodily perception, and a
40 sense of unity. Across 20 fMRI sessions, we measured functional connectivity in four
41 conditions (Baseline, Transition, NOC, and Residual) and compared the results with a
42 matched control group. During the Transition phase, connectivity became more variable,
43 indicating a temporary destabilization of network organization. In the NOC state, inter-
44 network connectivity decreased broadly, with visual cortex showing reduced coupling to
45 auditory, sensorimotor, orbitofrontal, thalamic, and cerebellar regions, and the somatomotor-
46 dorsal network disengaging from auditory and language cortices, paralleling the reported
47 visual phenomena and changes in bodily experience. In contrast, frontoparietal and salience
48 networks showed increased coupling with precuneus/posterior cingulate, multimodal
49 temporal cortex, and cerebellar hubs, in agreement with subjective reports of sustained
50 inward-directed attention and stable absorption. Entropy and complexity analyses revealed
51 systematic shifts that tracked the experiential sequence and returned to baseline in the
52 Residual condition. This single-case study brings together something uncommon: controlled
53 experimentation, voluntary induction of NOC states, and rich phenomenological data. Taken
54 together, these elements offer a strong foundation for neurophenomenological research and
55 illustrate why pairing structured paradigms with lived experience is useful for understanding
56 non-ordinary states of consciousness.

57

58

59

60

61

62

63

64

65

66

67

68

69

70 1. Introduction

71 Non ordinary states of consciousness (NOC), defined as mental states that differ
72 qualitatively from ordinary waking experience (Tart, 1976; Timmermann et al., 2023), arise
73 across a wide range of human experiences and are receiving increasing attention in
74 neuroscience (Fort et al., 2025; Gosseries et al., 2024). Pharmacologically induced NOC,
75 especially those obtained with anaesthetics and psychedelics, have been central to
76 identifying large scale neural signatures of NOC. These models, however, present several
77 limitations. Anaesthesia-based approaches often emphasise global markers of conscious
78 level rather than the structure of conscious contents. Psychedelic states pose different
79 challenges: the timing and trajectory of the experience cannot be easily controlled or aligned
80 across sessions or participants, the most intense phases tend to show reduced reportability,
81 and their overall reproducibility of phenomenology is very limited (Timmermann et al., 2023).
82 Also, pharmacological induction involves physiological changes caused by the drug itself,
83 which complicates the interpretation of neural effects (Bartfeld et al., 2015; Stamatakis et
84 al., 2010). Together, these limitations constrain the granularity with which phenomenology
85 can be related to neural dynamics and hinder efforts to link the richness of conscious
86 experience to its moment-to-moment neural organisation (Timmermann et al., 2022, 2023).

87 Voluntarily induced NOCs offer a complementary approach. Practices such as deep
88 absorption, meditative concentration, hypnosis and certain forms of trance show that some
89 individuals can intentionally enter NOCs while preserving awareness and moving through a
90 recognizable temporal progression (Berkovich-Ohana, 2015; Cardeña, 2005; Cardeña et al.,
91 2013; Deeley et al., 2013). These states make possible the study of NOC without
92 pharmacological perturbations and without loss of behavioural control. However, their
93 phenomenology often varies across episodes and across practitioners, and reproducibility at
94 the level of internal phases or trajectories has rarely been demonstrated, and the risk is to
95 study a collection of isolated, highly idiosyncratic states and to obtain neural correlates
96 without a coherent structure or predictive power. As a result, we still know little about the
97 neural dynamics that support their respective NOCs, and even less about their temporal
98 organisation.

99 This tension between models that offer strict experimental control at the cost of
100 phenomenological richness, and models that offer rich experiences at the cost of control and
101 reproducibility, has made it challenging to develop frameworks capable of mapping complex
102 experiences onto precise neural dynamics, the neurophenomenological goal. The present
103 study aims to address this gap by combining a systematic and reproducible framework,
104 organised into four defined and repeatable phases inspired by anaesthesia research

105 (Barttfeld et al., 2015; Chennu et al., 2016), with the experiential richness of a voluntary self-
106 induced NOC.

107 We examined a self-taught participant capable of intentionally entering a NOC state
108 that can be reliably reproduced across scanning sessions, with a phenomenology that
109 overlaps with features described in psychedelic, hypnotic and trance, such as visual
110 imagery, altered embodiment, shifts in time perception and ego attenuation. The state
111 includes features such as vivid internal imagery, alterations of body schema, changes in
112 agency and a sense of unity, while retaining a high degree of voluntary control and temporal
113 stability (Cardeña et al. 2025). Across four fMRI conditions (Baseline, Transition, NOC, and
114 Residual), we analysed functional connectivity and signal complexity, complemented by a
115 micro-phenomenological interview and detailed post-session reports. Based on the literature,
116 we hypothesised that the NOC state would involve reduced inter-network connectivity,
117 increased connectivity within frontoparietal and default mode systems, a rise in connectivity
118 variability during the transition phase and systematic changes in entropy and complexity
119 across conditions. Taken together, these elements provide an opportunity to examine how a
120 self-induced NOC reorganises large-scale brain dynamics across well-defined experiential
121 phases.

122

123 **2. Materials and methods**

124 **2.1. Participants**

125 The main participant is a 37-year-old woman (author AVP) with the ability to self-induce a
126 NOC known as a visionary transcendental state. This label, introduced by (Cardeña et al.,
127 2025), refers to a sequence of experiential modes within NOCs that progress from vivid
128 visionary imagery to transcendental or unitive awareness. Such states typically involve
129 luminous and often symbolically charged visual forms, heightened absorption with reduced
130 sensory input, dissolution of perceptual and ego boundaries, a sense of timelessness, and
131 an encompassing feeling of connection or merging with a larger reality. In AVP, this
132 trajectory unfolds spontaneously and reproducibly across sessions: it begins with intricate
133 geometric and luminous imagery and culminates in a lucid, expansive state of unity and
134 serenity, closely matching the phenomenological continuum described in the taxonomy. At
135 the time of data collection, she was not involved in the study design, hypothesis formulation,
136 data analysis, or interpretation. She was blinded to the specific aims of the study and
137 participated solely as a volunteer. All data preprocessing, connectivity analyses, and
138 statistical procedures were conducted independently by the research team and completed
139 before any results were shared with her. Her inclusion as an author reflects her substantial

140 contribution to the neurophenomenological interpretation of the findings, particularly through
141 detailed introspective reports and participation in a micro-phenomenological interview.

142 The absence of clinical criteria for psychiatric disorders (based on DSM-5-TR) was
143 confirmed through an open psychiatric interview (conducted by author SC). A semi-
144 structured interview was used to complete the Positive and Negative Syndrome Scale
145 (PANSS) (Kay et al., 1987), specifically aiming to rule out schizophrenia or other psychotic
146 disorders due to the presence of sensory-perceptual alterations. We ruled out anxiety
147 disorders, mood disorders, psychotic disorders, obsessive-compulsive spectrum disorders,
148 trauma-related disorders, dissociative disorders, sleep-wake disorders, conduct disorders,
149 substance-related disorders, personality disorders, neurodevelopmental disorders, and
150 medication-induced disorders. The participant was in good health and reported no medical
151 conditions other than compensated hypothyroidism treated with levothyroxine.

152 The participant did not receive formal training in techniques for inducing non-ordinary
153 states of consciousness. Her practice developed intuitively and independently from early
154 adolescence, as part of a sustained curiosity about the nature of perception and
155 consciousness. At age 24 she experienced a spontaneous visual phenomenon (a yellow
156 shape projected onto a blank surface) that she later learned to reproduce voluntarily through
157 self-guided experimentation. Over time, she progressively refined this ability through
158 reasoning and introspection, rather than through any specific contemplative or meditative
159 method. This practice has since become a continuous mode of perception and inquiry rather
160 than a discrete daily exercise. She also reports stable associations between letters,
161 numbers, and colors (e.g., perceiving "S" as yellow and "T" as green), consistent with mild
162 grapheme-color synesthesia present since childhood.

163 A control group of ten female volunteers, matched to AVP in age and level of
164 education (Table S1) was included. Controls met the same inclusion criteria (absence of
165 neurological or psychiatric conditions and overall good health), assessed through self-report
166 and brief interviews. All controls underwent the same MRI protocol as AVP. Participants
167 were recruited using snowball sampling through social media. All participants read and
168 signed the information and consent form provided by the ethics committee that approved the
169 project (Ethics Committee of the Institute of Psychological Research, CONICET Córdoba).
170 All data collections and analyses were carried out in accordance with the Declaration of
171 Helsinki.

172 **2.2. Psychological assessment**

173 AVP was interviewed multiple times by one of the authors with expertise in
174 phenomenological methods (EC). A micro-phenomenological interview (Petitmengin, 2006)
175 was conducted focusing on one of her experiences during scanning, using open-ended
176 questions (see Supplementary Information). In addition, AVP produced detailed written notes

177 after each session. These reports, summarized in Table S2, indicated consistent induction of
178 the core NOC with moderate session-specific variation.

179 **2.3. Brain imaging**

180 AVP completed 20 MRI sessions, each organized into four distinct blocks (Figure 1a).
181 Sessions were collected over a period of five months (March to July, 2023, with a typical
182 interval of one week between sessions. This number of sessions was chosen to obtain a
183 statistically meaningful sampling of both the stable and variable components of the self-
184 induced state, while remaining feasible for the participant, who committed to a demanding
185 schedule without compromising her well-being. All sessions were conducted under highly
186 comparable conditions (same time of day, same scanner environment, eyes closed at
187 rest). The participant reported stable induction ability across sessions, no signs of fatigue or
188 habituation, and no episodes of drowsiness or sleep.

189

190 A Siemens Spectra 3 Tesla MRI machine, with 16 channel head coil, was used to
191 obtain 36 ascending interleaved slices (TR = 3000 ms, TE = 30 ms, flip angle 90°). We also
192 collected T1-weighted structural images with 1x0.488x0.488 mm resolution, using an
193 MPRAGE sequence with TR = 1620 ms, TI = 900 ms, TE = 2.42 ms and flip angle = 9°.
194 Each session consisted of four functional blocks, each lasting 7:30 minutes, and a structural
195 block, organized as follows: the first block was a *Baseline* condition (common resting state),
196 the second block was labeled *Transition* (where AVP began to alter her mental state), the
197 third block was *NOC*, and the fourth block was *Residual* (AVP attempted to return to
198 Baseline but remained in a partially altered state that no longer matched the NOC yet had
199 not fully resolved into ordinary wakefulness). During Transition, AVP signaled having
200 crossed the subjective threshold into the NOC using a small foot movement. In the Residual,
201 she was asked to move her foot at a random moment to provide a control movement
202 condition. To ensure this did not affect analyses, connectivity was recomputed after
203 removing the three volumes before and after the movement; results were unchanged ($r =$
204 0.99; Figure S1).

205 Between blocks, an experimenter entered the MRI room to cue the next condition
206 except between the Transition and NOC to avoid distractions. The T1 image was collected
207 between the third and fourth blocks to allow recovery time.

208 Control participants followed the same protocol but were instructed to maintain eyes
209 closed and generate visual imagery during the second and third blocks (corresponding to
210 Transition and NOC in AVP). One control participant did not complete the Baseline; another
211 had corrupted data in the third block. Authors GDB, DSGR and PB collected all data.

212 **2.4. Image preprocessing**

213 Images were preprocessed using CONN (Whitfield-Gabrieli & Nieto-Castanon, 2012) version
214 21.a standard preprocessing pipeline. The steps applied were: realignment and unwarping
215 for motion correction, slice timing correction, corregistration to the T1 image, segmentation,
216 normalization to the standard MNI space, and smoothing at 8 mm FWHM. Denoising
217 included white-matter and CSF components and motion regressors using aCompCor,
218 followed by band-pass filtering (0.008 - 0.09 Hz) and linear detrending.

219 Functional images were parcelated into 300 spherical Regions of Interest (ROIs)
220 from the Greene Lab atlas (Seitzman et al., 2020), grouped into 14 functional networks
221 (Figure 1b). This atlas was selected because it provides fine-grained and anatomically well-
222 defined coverage of the entire brain, including cortical, subcortical, and cerebellar regions,
223 enabling whole-brain analyses of large-scale reconfigurations. Its explicit assignment of each
224 ROI to well-characterized networks makes it particularly suitable for quantifying intra- and
225 inter-network connectivity and for detecting network-specific modulations. This atlas labels
226 one of the networks and its 12 associated ROIs as “unassigned”. They were excluded from
227 all analyses leaving a total of 288 ROIs and 13 networks. The networks included in the atlas
228 are: dorsal attention (DA), medial temporal lobe (MTL), default mode network (DMN), reward
229 (Rew), salience network (SN), fronto-parietal (FP), somatomotor dorsal (SMD), somatomotor
230 lateral (SML), ventral attention (VA), cingulo-opercular (CO), visual (VIS), auditory (AUD) and
231 parieto-medial (PM). All analyses were conducted on the functional time series data from
232 these 288 ROIs.

233 **2.5. Connectivity per functional network**

234 We estimated the connectivity between and within functional networks. Except stated
235 otherwise, all 20 sessions were analyzed independently to estimate connectivity, entropy,
236 and complexity measures before averaging across sessions for each condition. For each
237 session and condition, we estimated brain connectivity by calculating the Pearson correlation
238 between pairs of time signals. This resulted in a 288 x 288 matrix per participant and
239 experimental condition (Figure 1c, d). We defined two types of connectivity: intra-network
240 (within the same network, averaging the correlation values of the submatrix corresponding to
241 a single network, Figure 2a, left) and inter-network (between regions of different networks,
242 averaging all correlation values of the submatrices corresponding to pairs of ROIs from one
243 network and all others, Figure 2a, right) and calculated each of them across the four
244 conditions (Figure 2b, c).

245 We calculated a normalized correlation, defined as the inter- or intra-network
246 correlation divided by the corresponding Baseline average (Figure 2d). Specifically, the inter-
247 network correlation is divided by the average inter-network correlation at Baseline, and,
248 similarly, the intra-network correlation is divided by the average intra-network correlation at
249 Baseline.

250 To gain a clearer understanding of the intra- and inter-network correlation dynamics,
251 we plotted each network's connectivity on a 2D plane (Figures 2 e-g and S3), with inter-
252 network correlation on the y-axis and intra-network correlation on the x-axis. Each point
253 represents an (intra, inter) pair correlation at the Baseline. We drew arrows from the
254 Baseline to the corresponding inter- and intra-network values for each condition. Longer
255 arrows indicate larger changes in correlation compared to the Baseline condition, and the
256 direction of the arrow illustrates whether the change was primarily in the inter- or intra-
257 network correlations.

258 We also used both the standard deviation (Figure 2h, top) and the coefficient of
259 variation (CV) (Figure 2h, bottom), calculated as the standard deviation of the average
260 correlation values per ROIs divided by their mean, for each subject or session and condition.
261 CV quantifies the relative variability of connectivity, providing a measure of the dispersion of
262 correlation values in relation to their mean. A high standard deviation or CV suggests that
263 the connections between brain regions are unstable and exhibit high variability, indicating
264 that functional connectivity in that condition or participant is inconsistent. Conversely, a low
265 CV suggests that the connections are more stable and consistent, with less relative
266 variability.

267 To compare connectivity changes across conditions, we calculated the differences
268 between the full 288-ROI correlation matrices for each condition. We then averaged these
269 differences within each network to obtain a single value per functional network. This value
270 represents the average difference in connectivity for that network between a given condition
271 and Baseline. We quantified these differences using both a mixed effects linear model and a
272 bootstrap procedure (see Statistical analysis section).

273 To visualize the spatial network distribution in a 2D plane, we constructed graphs for
274 each condition by binarizing the matrices, establishing the threshold as a number that
275 selected the strongest 1% of connections of each individual matrix. We used the Python
276 library NetworkX version 3.1 with the Kamada-Kawai algorithm (Kamada & Kawai, 1989), a
277 type of force-directed graph that aims to position nodes such that the edges have uniform
278 length and the vertices are uniformly distributed. The nodes corresponding to functional
279 networks whose connectivity changes across conditions were statistically significant were
280 colored using the FN's specific color, while the rest were colored gray to avoid visual
281 crowding.

282 To examine differences in network topology between Baseline and the rest of the
283 conditions, we computed binary global efficiency for each session. Each weighted matrix
284 was converted to an unweighted adjacency matrix by retaining only the top 5% strongest
285 connections, to ensure comparable network density across sessions and conditions.

286 Efficiency was then computed on these binarized graphs for all sessions and conditions. To
 287 statistically compare the two conditions, we used a Mann-Whitney U test.

288 We performed a seed-based connectivity analysis restricted to the ROIs that showed
 289 significant modulation in the previous analysis, grouped into four networks: two with
 290 decreased connectivity in the NOC state (VIS, SMD) and two with increased connectivity
 291 (FP, SN). For each participant and condition, we extracted the ROI time series and
 292 computed voxelwise connectivity maps using Pearson correlation, followed by Fisher z-
 293 transformation. For each network, the resulting z-maps from all its ROIs were averaged at
 294 the participant level to obtain a single connectivity map representing that network's whole-
 295 brain coupling pattern.

296 **2.6. Entropy and complexity**

297 The statistical complexity and permutation entropy (Bandt & Pompe, 2002) were calculated
 298 using the "ordpy" Python library (Pessa & Ribeiro, 2021). We applied the calculation over the
 299 BOLD time series of each subject, condition and ROI, using an embedding dimension of d=3
 300 and an embedding delay of tau=1, meaning that each symbol in the symbolic encoding was
 301 formed by considering three consecutive samples from the time series. We also evaluated
 302 alternative embedding parameters, including embedding dimensions of 2 and 4 and
 303 embedding delays of 1, 2, and 3. The analysis was performed both at the level of individual
 304 sessions and on time series obtained by concatenating all sessions within each condition. To
 305 compare between AVP's and control's entropy and complexity values we employed a
 306 bootstrap procedure (see section 2.7. Statistical analysis).

307 **2.7. Statistical analysis**

308 We applied mixed effects linear models implemented with the Python library Statsmodels,
 309 version 0.14.0. All reported p-values were corrected for multiple comparisons using a False
 310 Discovery Rate (FDR) correction with a 5% significance level, unless stated otherwise. For
 311 the inter-network and intra-network correlation models, we used the following formulas

$$312 \quad Ic \text{ Network} + Condition - 1 + (1 \vee Session)$$

$$313 \quad Ec \text{ Network} + Condition - 1 + (1 \vee Session)$$

314 where 'Ic' ('Ec') is the difference in intra-correlation (inter-correlation) between matrices from
 315 a given condition and the Baseline, 'Network' is a categorical variable encoding the network
 316 identity (1 to 13), and 'Condition' encodes the four experimental conditions: Baseline (BL),
 317 Transition (TR), NOC, and Residual (RES). 'Session' is a random effect variable
 318 representing the session number (1 to 20).

319 For the standard deviation and the CV we employed the models:

$$320 \quad CV \text{ Condition} + (1 \vee Session)$$

$$321 \quad STD \text{ Condition} + (1 \vee Session)$$

322 STD stands for standard deviation across correlation values from a single connectivity
 323 matrix. The conditions were compared to the Baseline (as we included the intercept) to
 324 observe differences in CV relative to the Baseline condition.

325 For the permutation entropy and statistical complexity we used the following models:

$$326 \quad PE \ Network + Condition - 1 + (1 \vee Session)$$

$$327 \quad SC \ Network + Condition - 1 + (1 \vee Session)$$

328 where PE is permutation entropy and SC is statistical complexity.

329 In order to select significant networks in Figure S4a we used the model:

$$330 \quad C \ Network - 1 + (1 \vee Session)$$

331 where C is the difference in connectivity between each condition and Baseline. For the
 332 analyses of network connectivity per significant network we employed the following model

$$333 \quad NC \ Condition - 1 + (1 \vee Session)$$

334 where NC is the network connectivity for the significant networks visual, somatosensory
 335 dorsal, fronto-parietal, salience Network, and ventral attention. Figure S4a plots the
 336 correlation values per condition for all significant networks.

337 In the difference in network connectivity analysis (Figure 4) we conducted three
 338 separate models:

$$339 \quad DT \ Network_{pair} - 1 + (1 \vee Session)$$

$$340 \quad DN \ Network_{pair} - 1 + (1 \vee Session)$$

$$341 \quad DR \ Network_{pair} - 1 + (1 \vee Session)$$

342 where DT represents the difference in network correlation between Transition and Baseline,
 343 DN represents the difference between NOC and Baseline, and DR represents the difference
 344 between Residual and Baseline. 'Network_pair' is a categorical variable representing the
 345 network pair (i.e., the networks i and j involved in each correlation value).

346 For the ROI connectivity analysis in Figure 5b we conducted three models:

$$347 \quad DT \ ROI - 1 + (1 \vee Session)$$

$$348 \quad DN \ ROI - 1 + (1 \vee Session)$$

$$349 \quad DR \ ROI - 1 + (1 \vee Session)$$

350 Statistically significant ROIs were divided into those that increased and those that
 351 decreased in connectivity in each condition and were plotted in Figure 5b.

352 We also compared AVP data with the control group. We implemented a
 353 bootstrapping procedure (Davison & Hinkley, 1997) for each of the four conditions and each
 354 measure (Inter, Intra, Variation Coefficient, and Network Pair connectivity). We combined
 355 each of the 20 values (one per session) from the AVP group with 10 values from the control
 356 group (one per participant). Since the control group had 2 participants with 1 condition where
 357 the values were NaNs (due to defects), we filtered out the NaN values and sampled with

358 replacement, in each iteration, until we obtained 20 values for the control group. The
359 difference between the averages of the measures for each group was calculated, and the
360 entire process was repeated 50,000 times to obtain a distribution of differences (referred to
361 as the null distribution). We compared the actual difference from the empirical data with this
362 null distribution: the probability of obtaining the actual difference under the null distribution is
363 the p-value associated with that measure and condition. The p-values were adjusted for
364 multiple comparisons using a FDR correction with a 5% significance level. To compare the
365 ROI-level connectivity between the AVP group and the control group, we identified the
366 significant ROIs in the AVP group, averaged them into a single value per session, and
367 compared these values against the corresponding ROIs in the control group using a
368 bootstrap procedure as described before.

369 For the parameter exploration in the entropy analysis we followed a similar approach.
370 Concatenation provided longer time series, allowing for more reliable estimates of the
371 underlying symbolic probability distributions and, consequently, of entropy and complexity.
372 However, concatenating sessions removed the possibility of applying statistical models. To
373 address this limitation, we implemented a bootstrap-based procedure. Specifically, we
374 generated 100 surrogate concatenated time series by randomly sampling and stitching
375 together sessions from both the Baseline and NOC. For each surrogate series, we computed
376 entropy and complexity, thus obtaining a null distribution that we approximated as normal
377 using its mean and standard deviation. We then compared the empirical difference,
378 computed from the actual concatenated Baseline and Alteration series (20 sessions each),
379 against this null distribution to derive a p-value.

380 For the seeds analysis we compared NOC versus Baseline using voxelwise paired t-
381 tests, applying FDR correction at $q < 0.05$, with a minimum cluster size of 10.

382 **3. Results**

383 **3.1. Psychological traits and states phenomenology**

384 The micro-phenomenological interview and session-by-session reports revealed a highly
385 structured and reproducible experiential sequence across the 20 fMRI sessions (Table 1). At
386 the beginning of each session, she entered the scanner in an ordinary mental mode,
387 engaging in everyday thoughts and concrete concerns. From this baseline, she intentionally
388 relaxed by scanning her body, loosening muscles, and allowing herself to feel progressively
389 lighter. The constant sound of the MRI scanner served as a stable anchor “like a mantra”
390 that facilitated attentional focusing rather than distracting her. The Transition phase was
391 effortful, unstable, and required active intention. This phase consistently began with the
392 emergence of violet coloration replacing the dark visual field, followed by the gradual
393 appearance of a yellow-violet hexagonal lattice perceived not as an inner image but as a

394 structured pattern “in the air” surrounding her. She emphasized a distinct sense of “double
 395 consciousness”: while fully aware of being inside the scanner, she simultaneously felt
 396 connected to a broader field of experience characterized by serenity, unity, and reduced
 397 fragmentation of time. Bodily sensations during this phase were notably variable: in some
 398 sessions she reported tension and instability, whereas in others she experienced marked
 399 lightness and a diffuse sense of expansion.

400 Upon entering the fully developed NOC, the experience stabilized into a vivid
 401 visionary mode accompanied by profound calmness, spatial expansion, and attenuated
 402 bodily boundaries. She reported an “eternal present,” a continuous temporal flow with
 403 minimal segmentation. Across sessions, the most stable phenomenological motif was the
 404 hexagonal network coupled with rhythmic violet pulses. As the state deepened, lucid dream-
 405 like scenes emerged: landscapes, horizons, and interactions with imagined figures felt vividly
 406 present. In one session, uncrossing her imagined legs produced a strikingly real bodily
 407 sensation despite complete physical immobility. Multisensory modulation was also common,
 408 particularly deliberate manipulation of the scanner’s pitch and timbre, which she described
 409 as stretching or modulating the sound “like gum.” In several sessions, she reported cubic
 410 grids, labyrinth-like structures, and highly organized geometric patterns resembling sacred
 411 geometry.

412 The Residual phase was triggered by the researcher’s entrance into the scanner
 413 room and unfolded gradually, aided by intentional movement. Although the visionary imagery
 414 dissipated quickly, she often remained in an expanded sensory mode for 30 to 60 minutes
 415 afterward, reporting heightened brightness, softened edges, and an extended sense of
 416 physical and mental openness.

417 The phenomenology was remarkably consistent across the 20 sessions. The
 418 hexagonal network and violet pulse appeared in every session, and most sessions featured
 419 variations of geometric structures, depth distortions, bodily expansion, or dream-like
 420 imagery. This reproducibility, together with the detailed micro-phenomenological account,
 421 supports the interpretation that AVP’s NOC is a stable, voluntarily accessible state with a
 422 well-defined experiential structure, suitable for systematic neurophenomenological
 423 investigation.

424 **3.2. Brain imaging**

425 **3.2.1. Global connectivity**

426 Intra-network connectivity decreased significantly compared to Baseline in both the NOC (β
 427 = -0.009, SE = 0.004, p = 0.038 FDR corrected) and Residual conditions (β = -0.009, SE =
 428 0.004, p = 0.038 FDR corrected) (Figure 2a, b), and inter-network connectivity decreased in
 429 all three conditions compared to the Baseline (Transition; β = -0.007, SE = 0.002, p < 0.001
 430 FDR corrected) (NOC; β = -0.005, SE = 0.002, p = 0.001 FDR corrected) (Residual; β = -

431 0.008, SE = 0.002, $p < 0.001$ FDR corrected) (Figure 2c). The comparison between AVP's
 432 results and those of the control group also revealed significant differences, both for inter-
 433 network (Baseline v. Transition; $p = 0.002$, FDR corrected) (Baseline v. NOC; $p = 0.01$ FDR
 434 corrected) and intra-network connectivity (Baseline v. NOC; $p = 0.01$ FDR corrected)
 435 (Baseline v. Residual; $p = 0.01$). We found no difference between conditions in the control
 436 group (Figure S2a, left, right) except in the inter connectivity for NOC v. Baseline but with the
 437 opposite effect ($\beta = 0.019$, SE = 0.008, $p = 0.043$ FDR corrected) (Figure S2a, middle).

438 Intra-network connectivity showed no variations across states, whereas the most
 439 robust effects were observed in inter-network connectivity during the Transition ($\beta = -0.295$,
 440 SE = 0.134, $p = 0.04$ FDR corrected) and Residual ($\beta = -0.345$, SE = 0.134, $p = 0.03$ FDR
 441 corrected) conditions (Figure 2d). Inter-network connectivity decreased relative to Baseline
 442 during Transition and Residual, suggesting a reorganization of the existing networks rather
 443 than a dissolution of the networks observed during normal wakefulness. In the control group,
 444 the only statistically significant difference was observed between NOC and Baseline
 445 conditions ($\beta = 0.645$, SE = 0.264, $p = 0.03$ FDR corrected), where normalized inter-network
 446 connectivity was higher during Baseline than in NOC, an effect opposite to that observed in
 447 AVP (Figure S2b).

448 Figure 2e-g shows the plots with intra-network connectivity on the x-axis and inter-
 449 network connectivity on the y-axis. The base or starting point of each vector is the intra-inter
 450 pair of the Baseline, and the arrowhead or endpoint is the specific pair of the graphed
 451 condition. Some networks vary greatly in their connectivity while others change very little,
 452 suggesting that the changes associated with AVP's phenomenological states are network-
 453 specific. In particular, the visual and somatosensory networks strongly decrease their inter-
 454 network connectivity, while frontoparietal network connectivity increases monotonically
 455 across conditions (Figure 2 e-g). In the Transition vs. Baseline comparison, we observed
 456 only one functional network that significantly changed: the visual network, which decreased
 457 its connectivity ($\beta = -0.025$, $p < 0.001$). In NOC vs. Baseline comparison, three networks
 458 significantly decreased their connectivity: the visual network ($\beta = -0.032$, $p < 0.001$), the
 459 ventral attention network ($\beta = -0.017$, $p = 0.048$), and the sensorimotor dorsal network ($\beta = -$
 460 0.024, $p = 0.018$) and one increased its connectivity: the frontoparietal network ($\beta = 0.018$, p
 461 = 0.019). In Residual vs. Baseline, the visual network ($\beta = -0.032$, $p < 0.001$), the ventral
 462 attention network ($\beta = -0.010$, $p = 0.013$), and the sensorimotor dorsal network ($\beta = -0.035$, p
 463 < 0.001) all decreased their connectivity, while the salience network ($\beta = 0.018$, $p = 0.0094$)
 464 increased its connectivity. In the control group, no significant differences were observed
 465 between conditions in either intra- or inter-network connectivity (Figure S3), and none of the
 466 connectivity changes seen in AVP were replicated.

467 Standard deviation increased significantly specifically in the Transition (Transition v.
 468 Baseline; $\beta = -0.009$, SE = 0.004 p = 0.03 FDR corrected) and this increment was specific to
 469 the Transition (Transition v. NOC, $\beta = -0.008$, SE = 0.004 p = 0.047 FDR corrected)
 470 (Transition v. Residual, $\beta = -0.011$, SE = 0.004 p = 0.013 FDR corrected) (Figure 2h, top).
 471 This shows that the standard deviation values were higher during the Transition compared to
 472 Baseline, indicating increased global variability. Comparing AVP to controls, this increment
 473 showed no significance (Baseline v. Transition; p = 0.24) (Transition v. NOC; p = 0.07)
 474 (Transition v. Residual; p = 0.09). We also found that the coefficient of variation increased
 475 significantly in all conditions (Baseline v. Transition; $\beta = 1.823$, SE = 0.774, p = 0.018 FDR
 476 corrected) (Baseline v. NOC; $\beta = 1.889$, SE = 0.774, p = 0.018 FDR corrected), (Baseline v.
 477 Residual; $\beta = 2.146$, SE = 0.774, p = 0.016 FDR corrected) (Figure 2h, bottom) and
 478 comparing AVP to controls all conditions were close but not significant (Baseline v.
 479 Transition; p = 0.055) (Baseline v. NOC; p = 0.055) (Baseline v. Residual; p = 0.055).

480 **3.2.2. Entropy and complexity**

481 The entropy analysis showed significantly lower values in the Transition compared to
 482 Baseline ($\beta = -0.0129$, SE = 0.0003, p < 0.001, FDR corrected) and to NOC ($\beta = -0.0169$, SE
 483 = 0.0003, p < 0.001, FDR corrected) (Figure 3a). Similarly, statistical complexity also
 484 exhibited a significantly higher value in Transition ($\beta = 0.0010$, SE = 0.0002, p < 0.001, FDR
 485 corrected) and NOC ($\beta = 0.0013$, SE = 0.0002, p < 0.001, FDR corrected) as compared to
 486 Baseline (Figure 3b). In contrast, no statistically significant differences were observed
 487 between the Baseline and Residual for either entropy or complexity. The entropy-complexity
 488 plane (Figure 3c) provides a clear visualization of the dynamic shifts in brain activity across
 489 conditions. We found significant differences between AVP and the control group only in the
 490 Baseline vs. Residual conditions for both entropy (p = 0.008, FDR corrected) and complexity
 491 (p = 0.016, FDR corrected). When we varied the embedding parameters away from the
 492 canonical configuration ($d = 3$, $\tau = 1$), we found no statistically significant differences
 493 between Baseline and NOC (Figure S5). Concatenating all sessions into a single timeseries
 494 for each condition (Figure S6) we observed statistically significant differences between
 495 Baseline and NOC for all combinations of embedding dimension and delay ($d=2$, $\tau=1$, p <
 496 0.001; $d=4$, $\tau=1$; p < 0.001; $d=3$, $\tau=2$, p < 0.001; $d=3$, $\tau=3$, p < 0.001).

497 **3.2.3. Network-level analyses**

498 Focusing on the five networks that showed significant effects (visual, somatosensory
 499 dorsal, ventral attention, fronto-parietal, and salience), we observed network-specific
 500 connectivity changes across conditions in AVP (Figure S4a), with the visual and
 501 somatosensory dorsal networks consistently showing decreased connectivity, and the fronto-
 502 parietal network showing increased connectivity during the NOC state. Comparisons with

503 controls confirmed that these effects were specific to AVP (Figure S4b). Complete statistics
 504 are reported in the Supplementary Material.

505 We found that several connections changed during Transition, NOC, and Residual
 506 (Figure 4). The overall picture shows that the visual network appears to alter its connections
 507 the most, particularly with the ventral attention, auditory, and sensorimotor networks (i.e., the
 508 sensory and attentional networks) (see Table S3 for the complete list of network pairs). In
 509 the control group, no significant differences were found between conditions (see Table S4
 510 for the complete list of network pairs).

511 **3.2.4. ROI-level analyses**

512 NOC state significantly differed from Baseline in network efficiency ($U = 126$, $p =$
 513 0.046) with NOC showing higher values (mean efficiency = 0.344) than Baseline (mean
 514 efficiency = 0.335). However, we did not find significant differences between Baseline and
 515 Transition ($U = 244$, $p = 0.24$) or between Baseline and Residual ($U = 139$, $p = 0.10$). When
 516 comparing the conditions within the control group we found no statistically significant
 517 differences between Baseline and the rest of the conditions (Baseline vs. Transition: $U = 61$,
 518 $p = 0.42$; Baseline vs. NOC: $U = 55$, $p = 0.73$; Baseline vs. Residual: $U = 85$, $p = 0.53$). ROI-
 519 level analyses (Figure 5b; Table S5) showed no increases in connectivity during Transition,
 520 but several decreases, particularly in visual, cingulo-opercular, and sensorimotor areas. This
 521 disconnection pattern intensified in the NOC state and extended to dorsal and ventral
 522 attention ROIs, while a subset of frontoparietal ROIs showed increased connectivity. No
 523 significant connectivity differences across conditions were found in the control group.
 524 Compared to the control group, AVP showed significantly different ROI-level connectivity
 525 patterns during Transition (decreased connectivity, $p = 0.03$, FDR-corrected) and NOC
 526 conditions (both increases and decreases, $p = 0.03$, FDR-corrected, for each). No significant
 527 differences were observed in the Residual condition.

528 Seed-based connectivity of the visual network during the NOC state showed large-scale
 529 decreases relative to Baseline (Figure 6a). We found reduced coupling with bilateral
 530 temporal cortex (superior and middle temporal gyri, including Heschl's gyrus and opercular
 531 regions), postcentral and precentral sensorimotor cortices, inferior orbitofrontal cortex,
 532 limbic-parahippocampal regions, the thalamus (pulvinar and posterior nuclei), and extensive
 533 portions of the posterior cerebellum. No voxel showed increased connectivity at statistical
 534 threshold. A complete report of significant clusters can be found in Table S6.

535 The SMD network showed a similar pattern of disconnection during NOC (Figure 6b).
 536 We found decrements in connectivity with bilateral auditory and language cortices, including
 537 superior and middle temporal gyri, Heschl's gyrus, the planum temporale, Rolandic
 538 operculum, insula, and inferior frontal gyrus, indicating a general decoupling between SMD

539 and the language network, among other regions. No voxel showed increased connectivity at
 540 statistical threshold. A complete report of significant clusters can be found in Table S7.

541 FP connectivity conversely increased, in agreement with our previous analyses
 542 (Figure 6c). We found increased connectivity with precuneus and posterior cingulate,
 543 bilateral middle and inferior temporal cortices, precentral and supplementary motor regions,
 544 medial prefrontal cortex, and extensive portions of the posterior cerebellum. No voxel
 545 showed decreased connectivity at statistical threshold. A complete report of significant
 546 clusters can be found in Table S8.

547 SN also increases its connectivity (Figure 6d), particularly with precuneus/posterior
 548 cingulate, lingual and calcarine cortex, anterior cingulate, bilateral basal ganglia, thalamus,
 549 and posterior cerebellum, indicates a broad strengthening with regions involved in internal
 550 monitoring and multisensory integration. No voxel showed decreased connectivity at
 551 statistical threshold. A complete report of significant clusters can be found in Table S9.

552

553 4. Discussion

554 4.1. Summary of main findings

555 In this study, we examined the neurophenomenology of a self-induced NOC by integrating
 556 first-person reports with repeated measures of brain activity. Unlike most empirical
 557 approaches based on pharmacological manipulations or pathological conditions, this non-
 558 pharmacological and volitionally induced a structured, reproducible sequence of experiential
 559 phases while preserving full awareness. This design enabled a detailed examination of how
 560 systematic changes in experience correspond to large-scale neural dynamics across 20
 561 independent sessions. Our analytic framework was guided by four hypotheses derived from
 562 research on psychedelic, meditative, and hypnotic states (Cardeña et al., 2013; Carhart-
 563 Harris et al., 2012; Dor-Ziderman et al., 2016; Gosseries et al., 2024; Lanfranco et al., 2021;
 564 Lewis-Healey et al., 2024; Mainieri et al., 2017; Smigelski et al., 2019; Stoliker et al., 2024;
 565 Tagliazucchi et al., 2016; Timmermann et al., 2023). Below, we discuss each hypothesis in
 566 relation to the present findings.

567 4.2. Evaluation of the four hypotheses

568 Hypothesis 1 predicted reduced inter-network connectivity during NOC. This prediction was
 569 strongly supported: dorsal somatomotor, visual, and ventral attention networks showed
 570 pronounced decoupling relative to Baseline. In the control group, the modest but significant
 571 increase in inter-network connectivity observed in the NOC condition likely reflects non-
 572 specific fluctuations in vigilance or spontaneous imagery rather than a structured state
 573 change, consistent with prior reports of transient increases in large-scale correlations during
 574 relaxed wakefulness and early drowsiness (Tagliazucchi & van Someren, 2017).

575 AVPs reduced inter-network visual connectivity during NOC resonates with her
576 intense and highly structured visual phenomena, including a recurring yellow hexagonal grid,
577 violet pulses, and fractal-like imagery. Such geometric imagery has been described in
578 entoptic and drug-induced visual research (Miyashita, 1995; Siegel, 1977; Siegel & Jarvik,
579 1975), and computational models suggest that these lattice-like percepts arise from intrinsic
580 excitatory and inhibitory interactions in early visual cortex when sensory input is reduced and
581 cortical excitability increases (Bressloff et al., 2001, 2002; Ermentrout & Cowan, 1979). Also,
582 the pronounced decoupling of somatomotor and ventral attention networks indicates a
583 functional disengagement from external sensory input and bodily orientation, consistent with
584 AVP's descriptions of reduced boundaries and immersive visual absorption. Reduced
585 recruitment of the ventral attention network, which normally detects external salience and
586 reorients attention, likely reflects a shift toward internally maintained imagery, while
587 somatomotor decoupling aligns with attenuation of proprioception and affected body
588 perception. Together, these results point to a reorganization of large-scale functional
589 architecture that favors internally driven and symbolically rich experiential content.

590 The visual seed showed that the visual network became more segregated during the
591 NOC state, with reduced connectivity to sensorimotor, auditory, orbitofrontal, and thalamic
592 regions. This pattern matches the participant's reports of vivid internal imagery, diminished
593 orientation to external input, and a weaker sense of bodily and auditory anchoring. The
594 decreases in visuo-auditory and visuo-sensorimotor coupling, together with the
595 disconnection from posterior cerebellum and pulvinar, fit well with accounts of "closed-loop"
596 visual cortex dynamics and with models in which geometric imagery arises from intrinsic self-
597 organization within early visual areas. These results indicate a shift toward predominantly
598 endogenous visual processing, consistent with observations from psychedelic research
599 where visual regions become more autonomous and internally driven (Carhart-Harris et al.,
600 2016; Huels et al., 2021; Roseman et al., 2018) and with reports of sensory down-weighting
601 in deep meditative absorption (Ganesan et al., 2024; Yang et al., 2023).

602 The SMD seed analysis showed a clear decoupling from auditory and language-
603 related cortices, including bilateral STG/MTG, Heschl's gyrus, opercular regions, and inferior
604 frontal gyrus. This large-scale disengagement suggests a temporary suspension of the
605 audio-motor loop that normally supports speech, verbal imagery, and auditory prediction.
606 The finding is consistent with the participant's reduced internal dialogue, altered sense of
607 bodily anchoring, and voluntary modulation of scanner sounds.

608 Hypothesis 2 predicted increased connectivity within frontoparietal and default mode
609 networks. This hypothesis was partially supported. We found a significant increase in FP
610 connectivity during the NOC, which returned to baseline during recovery. This pattern is
611 consistent with AVP's descriptions of heightened awareness, cognitive clarity, and

612 intentional engagement with inner experience. The salience network also showed early and
613 sustained increases, particularly in the dACC, thalamus, and insula, which may reflect
614 enhanced interoceptive and attentional regulation (Quigley et al., 2021; Salomon et al.,
615 2016; Tsakiris & Critchley, 2016). However, DMN connectivity did not show significant
616 changes, diverging from prior findings in psychedelic research (Gattuso et al., 2023), which
617 reported decreases in within-DMN and increases in DMN-inter-network connectivity.
618 Consistent with this distinction, our seed analysis revealed no increases within the DMN
619 itself, but showed clear cross-network strengthening between FP and posterior midline DMN
620 hubs (precuneus/posterior cingulate) during NOC. This difference likely reflects the distinct
621 nature of the two states: psychedelic experiences are pharmacologically induced and often
622 associated with profound ego dissolution, whereas AVP's state was self-induced and stable.
623 Similar patterns have been reported in non-pharmacological NOC such as shamanic trance,
624 auto-induced cognitive trance, and deep absorption, where vivid imagery and sensory
625 attenuation occur without disintegration of the DMN or loss of self (Grégoire et al., 2024;
626 Hove et al., 2016; Huels et al., 2021; Yang et al., 2023). These characteristics may sustain a
627 balanced engagement of self-referential and control processes, preventing the DMN
628 disintegration typically observed under psychedelics. Thus, rather than a collapse or
629 hyperintegration of the DMN, AVP's state may involve a dynamic reorganization that
630 preserves introspective awareness within a stable network architecture, supported by
631 selective increases in FP–DMN coupling rather than global DMN modulation.

632 The frontoparietal seed showed increased connectivity with the precuneus/posterior
633 cingulate, medial prefrontal cortex, temporal multimodal regions, precentral/SMA areas, and
634 posterior cerebellum. This configuration corresponds to a network known to support
635 internally focused attention, scene construction, visuospatial imagery, and sensorimotor
636 prediction. The strengthening of FP-precuneus coupling is particularly notable, as similar
637 patterns have been observed in states of sustained internal absorption (Hasenkamp et al.,
638 2012) and in high-field intensive-sampling meditation studies demonstrating enhanced FP-
639 midline integration during deep concentration (Yang et al., 2023). This aligns closely with the
640 participant's descriptions of vivid internal scenes, stable inward-directed focus, and the
641 feeling of "being inside" a visual environment (Grégoire et al., 2024; Huels et al., 2021).

642 Finally, the salience network showed increased connectivity during the NOC state,
643 especially with the precuneus/posterior cingulate, lingual and calcarine cortex, anterior
644 cingulate, basal ganglia, thalamus, and cerebellar Crus. This pattern suggests enhanced
645 interoceptive monitoring, subcortical regulation, and integration of internally generated visual
646 and mnemonic content. The coupling with posterior midline and early visual regions is
647 consistent with the participant's geometric imagery, depth sensations, and sustained inward
648 attention. Similar salience-driven stabilization of internally oriented states has been reported

649 in shamanic trance, auto-induced cognitive trance, and states of deep meditative absorption
650 (Gosseries et al., 2024; Hove et al., 2016; Mainieri et al., 2017).

651 Hypothesis 3 predicted increased variability during the Transition. The data strongly
652 supported this prediction, as we observed a marked increase in the variability of functional
653 connectivity, both in absolute terms and relative to the mean. This heightened variability was
654 especially prominent in the salience and frontoparietal networks, and diminished once the
655 NOC stabilized. AVP described this phase as effortful and disorganized, involving bodily
656 tension, active searching, and a sense of cognitive turbulence. Once she crossed a self-
657 identified threshold that marked the entry into the NOC this tension dissolves, giving way to
658 a stable and effortless experiential mode in which she reports being able to remain
659 indefinitely, as she does in her everyday life. These findings align with Tart's (1976) proposal
660 that transitions into NOC states involve temporary disorganization followed by the
661 emergence of a new experiential order. They also support recent models emphasizing
662 increased network flexibility and metastability as markers of non-ordinary states (Cabral et
663 al., 2022; Cavanna et al., 2018; Tagliazucchi & van Someren, 2017), suggesting that
664 transient neural destabilization may be a necessary condition for accessing alternate modes
665 of conscious experience.

666 Unexpectedly, although entropy and complexity depend only on the ordinal structure
667 of the BOLD signal rather than its amplitude, they also exhibited substantial variability across
668 sessions. This pattern likely reflects the combined influence of two factors. First, the
669 relatively short duration of each block (150 volumes) makes entropy and complexity
670 estimates less stable across runs. Second, and more importantly, while the participant
671 reported a consistent experiential core, she also described subtle variations in depth,
672 vividness, and immersion across sessions. These fine-grained phenomenological
673 fluctuations may be captured more directly by entropy and complexity-based metrics than by
674 connectivity measures, which integrate over slower timescales. In line with this
675 interpretation, entropy and complexity were also the only measures that fully returned to
676 baseline during the Residual phase, suggesting that they are particularly sensitive to the
677 stabilization and dissolution of the NOC.

678 Hypothesis 4 predicted systematic entropy and complexity changes. This was
679 confirmed: we observed decreased entropy and increased statistical complexity during both
680 Transition and NOC compared to Baseline, indicating a shift toward neural dynamics that are
681 more structured yet less stochastic. These changes reversed in the Residual phase,
682 suggesting that the brain's information-processing architecture flexibly reconfigures in
683 response to the NOC and can return to its Baseline organization even though AVP continued
684 to experience a residual form of the state. Notably, entropy and complexity were the only

685 measures that fully returned to baseline levels during Residual, underscoring their sensitivity
686 to the stabilization and subsequent dissolution of the NOC.

687 From a theoretical perspective, these findings suggest that the observed decrease in
688 entropy and increase in complexity may reflect a transient relaxation of stable network
689 configurations, allowing new patterns of conscious content to emerge. Such temporary
690 reorganizations could represent a flexible rebalancing between top-down constraints and
691 bottom-up dynamics, supporting the emergence of novel experiential structures. In this view,
692 increased complexity reflects the emergence of richly differentiated patterns of brain activity,
693 while reduced entropy suggests a departure from the high-noise regime of unconstrained
694 cognition toward a metastable, self-organizing mode (Cavanna et al., 2018; Coppola et al.,
695 2022; Mateos et al., 2018; Mindlin et al., 2024). This entropic trajectory may support the
696 phenomenological qualities reported by AVP, such as enhanced insight, symbolic
697 integration, and the dissolution of conventional perceptual and temporal boundaries.

698 **4.3. Convergences with meditation, trance, and psychedelic research**

699 Research on trance and related non-ordinary states provides convergent evidence for
700 structured reorganization of large-scale networks. fMRI and EEG studies of shamanic and
701 mediumistic trance (Hove et al., 2016; Huels et al., 2021; Mainieri et al., 2017) consistently
702 report increased coupling among hubs of the default mode and control networks, particularly
703 PCC, dACC, and insula, together with reduced connectivity in sensory pathways such as
704 auditory cortex. This pattern reflects a shift toward amplified internally oriented processing
705 and partial decoupling from exteroception. A comparable configuration appears in AVP's
706 NOC state, where visual, somatosensory, and ventral attention networks showed marked
707 disconnection, while frontoparietal and salience networks strengthened (Rogerson et al.,
708 2021). Phenomenological reports from auto-induced cognitive trance (AICT) and
709 Mahorikatan practices (Grégoire et al., 2024; Oswald et al., 2025; Vanhaudenhuyse et al.,
710 2024) describe vivid imagery, proprioceptive alterations, absorption, and narrowed external
711 orientation-features that partially overlap with AVP's experience. Trance studies repeatedly
712 highlight a pattern of sensory attenuation together with intensification of internally generated
713 experience, a combination that provides a strong external validation for the network
714 configuration observed in our data. Also, Studies of deep absorption (Ganesan et al., 2024;
715 Yang et al., 2023) show highly reliable within-subject modulation of sensory cortices,
716 attentional hubs, and subcortical structures. These convergences suggest that sensory
717 attenuation and heightened internal integration may represent general organizational motifs
718 across non-pharmacological NOC, even when their induction methods and cultural contexts
719 differ.

720 Together with trance and meditation research, these findings converge on a growing
 721 view that non-pharmacological NOC states are characterized by coherent yet reorganized
 722 network architectures, combining sensory decoupling with strengthened control and salience
 723 engagement, and exhibiting stable within-subject trajectories over time. This situates AVP's
 724 case within a broader class of intentional NOC that share both phenomenological structure
 725 and reproducible neural dynamics.

726 **4.4. Linking networks changes and AVP reports**

727 Table 1 summarizes the four experimental phases by aligning AVP's subjective reports with
 728 the corresponding large-scale network patterns. Baseline is characterized by ordinary
 729 mentation, intact bodily awareness, and a stable sensory frame, accompanied by typical
 730 intra- and inter-network connectivity, low variability, and high-entropy/low-complexity
 731 dynamics. During the Transition, AVP reports bodily tension, unstable attention, and the first
 732 appearance of geometric imagery in the form of honeycombs and violet pulses of light; this
 733 phase matches a peak in global variability (high STD and CV), early network decoupling
 734 especially in visual, cingulo-opercular, and somatomotor-dorsal regions, and a drop in
 735 entropy coupled with an increase in complexity. The NOC state corresponds to a stable,
 736 effortless immersive mode with vivid internal imagery, reduced proprioceptive grounding,
 737 and sustained inward focus; neurally, this aligns with strong inter-network decoupling in VIS,
 738 SMD, and VA, isolation of the visual system, disengagement of language network from SMD
 739 and increased FP and SN coupling with posterior midline and sensory hubs such as
 740 PCC/posterior cingulate, together with the lowest entropy and highest complexity. Finally,
 741 the Residual phase combines partial return to ordinary mentation with lingering perceptual
 742 and bodily alterations, mirrored by partial reconnection of networks, persistent reductions in
 743 inter-network connectivity (mainly VIS, VA, SMD), and a full return of entropy and complexity
 744 to baseline levels.

745 It is worth noting that AVP presents lifelong synesthetic traits, characterized by
 746 consistent cross-modal associations between sensory and affective modalities. Rather than
 747 confounding the present findings, this feature may help contextualize them. Synesthesia
 748 reflects a stable neurocognitive organization marked by increased structural and functional
 749 coupling across sensory association areas-patterns that may facilitate the emergence of
 750 vivid, multimodal imagery and fluid perceptual integration during non-ordinary states. In this
 751 light, AVP's synesthetic predisposition could have amplified the integrative and high-entropy
 752 dynamics observed in the visionary condition, offering a natural model of how enduring
 753 neural architectures interact with transient reorganizations of consciousness.

754 **4.5. Limitations**

755 This study has several limitations. First, the proposed experiential stages remain coarse
 756 approximations. Although they capture major transitions, more granular tracking, such as

real-time experience sampling, would improve temporal resolution and allow finer alignment between subjective reports and neural changes (Stawarczyk et al., 2011). Moreover, not all sessions were phenomenologically identical; subtle variations across NOC states could be better captured by increasing the number of sessions and examining recurring experiential features in more detail—for instance, identifying neural correlates of the reported out-of-body experiences. Second, only a single formal micro-phenomenological interview was conducted, despite AVP undergoing 20 sessions. However, this was complemented by detailed self-reports after each session, which showed strong consistency with the interview and support the reproducibility of the experiential pattern across sessions. While these reports allowed us to interpret certain neural changes in light of recurring experiential features, we acknowledge that these interpretations are experience-informed inferences, not formally tested correlations. This limits the strength of claims linking specific phenomenological content to particular network-level dynamics. Third, control participants did not provide structured post-scan interviews. However, all were asked open-ended questions after scanning, following standard resting-state protocols to ensure they had not fallen asleep or entered unintended mental states. All reported typical mentation, such as imagining everyday scenes or recalling recent events. Fourth, the exclusive use of fMRI limits temporal precision and may overlook fast neural transitions. Future studies could incorporate EEG or MEG to capture rapid shifts, particularly during threshold-crossing events, which AVP describes as nearly instantaneous. These additions would enable a more temporally resolved understanding of the dynamics underlying voluntary NOC induction. Finally, as this is an in-depth single-case study, the findings are not statistically generalizable to the wider population. AVP's ability to reliably and volitionally induce a specific NOC, while maintaining a clear and continuous sense of self and full awareness of the context, is rare and may not represent typical NOC experiences. Our interpretations are constrained by the uniqueness of her profile and the absence of replication in other individuals. Rather than offering generalizable conclusions, this study aims to generate hypotheses, demonstrate methodological possibilities, and contribute conceptually to the neurophenomenology of consciousness. The case demonstrates how subjective and neural data can be integrated to study complex experiential states in detail, but further work across diverse participants and contexts is needed to establish broader principles. We hope this work encourages both caution in extrapolation and curiosity about the heterogeneity of NOC experiences.

4.6. Conclusions

This study demonstrates how a self-induced NOC can be characterized as a coherent yet reorganized mode of conscious experience, with reproducible large-scale signatures tightly aligned with a phenomenological sequence. It highlights the value of integrating first-person reports with network-based neuroimaging and suggests that volitional modulation of

794 consciousness may reveal general principles of brain dynamics across diminished and
795 expanded states of awareness.

796

797 **5. Acknowledgements**

798 This research was supported by Agencia Nacional de Promoción Científica y Tecnológica,
799 Argentina (Grants #2018-03614 and CAT-I-00083). We thank the three anonymous
800 reviewers and the Guest Editors for their constructive feedback and thoughtful suggestions,
801 which significantly improved the clarity and scope of the manuscript. The authors used
802 ChatGPT to assist with English grammar editing. All scientific content, analyses, and
803 interpretations were written, reviewed, and approved by the authors.

804

805 **6. Data and code availability**

806 Data not publically available but it can be shared upon reasonable request.
807 The code used to analyze the data and generate the results is available at
808 <https://github.com/dellabellagabriel/visionary-state>. For further inquiries, please contact the
809 corresponding authors.

810

811 **7. References**

- 812 Bandt, C., & Pompe, B. (2002). Permutation Entropy: A Natural Complexity Measure
813 for Time Series. *Physical Review Letters*, 88(17), 174102.
<https://doi.org/10.1103/PhysRevLett.88.174102>
- 814 Barttfeld, P., Bekinschtein, T. A., Salles, A., Stamatakis, E. A., Adapa, R., Menon, D.
815 K., & Sigman, M. (2015). Factoring the brain signatures of anesthesia concentration
816 and level of arousal across individuals. *NeuroImage: Clinical*, 9, 385–391.
<https://doi.org/10.1016/j.nicl.2015.08.013>
- 817 Berkovich-Ohana, A. (2015). A case study of a meditation-induced altered state:
818 Increased overall gamma synchronization. *Phenomenology and the Cognitive
819 Sciences*, 1(16), 91–106. <https://doi.org/10.1007/s11097-015-9435-x>
- 820 Bressloff, P. C., Cowan, J. D., Golubitsky, M., Thomas, P. J., & Wiener, M. C. (2001).
821 Geometric visual hallucinations, Euclidean symmetry and the functional architecture

of striate cortex. *Philosophical Transactions of the Royal Society of London. Series B: Biological Sciences*, 356(1407), 299–330. <https://doi.org/10.1098/rstb.2000.0769>

Bressloff, P. C., Cowan, J. D., Golubitsky, M., Thomas, P. J., & Wiener, M. C. (2002). What Geometric Visual Hallucinations Tell Us about the Visual Cortex. *Neural Computation*, 14(3), 473–491. <https://doi.org/10.1162/089976602317250861>

Cabral, J., Castaldo, F., Vohryzek, J., Litvak, V., Bick, C., Lambiotte, R., Friston, K., Kringelbach, M. L., & Deco, G. (2022). *Synchronization in the connectome: Metastable oscillatory modes emerge from interactions in the brain spacetime network* [Preprint]. Neuroscience. <https://doi.org/10.1101/2022.01.06.475196>

Cardeña, E. (2005). THE PHENOMENOLOGY OF DEEP HYPNOSIS: QUIESCENT and Physically Active. *International Journal of Clinical and Experimental Hypnosis*, 53(1), 37–59. <https://doi.org/10.1080/00207140490914234>

Cardeña, E., Berkovich-Ohana, A., Valli, K., Barttfeld, P., Gomez-Marin, A., Greysen, B., Kumar, V. K., Laureys, S., Luhrmann, T. M., Newberg, A., Preller, K. H., Putnam, F. W., Tagliazucchi, E., Walsh, R., Carter, O., & Yaden, D. (2025). A consensus taxonomy of altered (nonordinary) states of consciousness: Bringing order to disarray. *Psychology of Consciousness: Theory, Research, and Practice*. <https://doi.org/10.1037/cns0000431>

Cardeña, E., Jönsson, P., Terhune, D. B., & Marcusson-Clavertz, D. (2013). The neurophenomenology of neutral hypnosis. *Cortex*, 49(2), 375–385. <https://doi.org/10.1016/j.cortex.2012.04.001>

Carhart-Harris, R. L., Erritzoe, D., Williams, T., Stone, J. M., Reed, L. J., Colasanti, A., Tyacke, R. J., Leech, R., Malizia, A. L., Murphy, K., Hobden, P., Evans, J., Feilding, A., Wise, R. G., & Nutt, D. J. (2012). Neural correlates of the psychedelic state as determined by fMRI studies with psilocybin. *Proceedings of the National Academy of Sciences*, 109(6), 2138–2143. <https://doi.org/10.1073/pnas.1119598109>

Carhart-Harris, R. L., Muthukumaraswamy, S., Roseman, L., Kaelen, M., Droog, W., Murphy, K., Tagliazucchi, E., Schenberg, E. E., Nest, T., Orban, C., Leech, R.,

- 852 Williams, L. T., Williams, T. M., Bolstridge, M., Sessa, B., McGonigle, J., Sereno, M.
853 I., Nichols, D., Hellyer, P. J., ... Nutt, D. J. (2016). Neural correlates of the LSD
854 experience revealed by multimodal neuroimaging. *Proceedings of the National
855 Academy of Sciences*, 113(17), 4853–4858.
856 <https://doi.org/10.1073/pnas.1518377113>
- 857 Cavanna, F., Vilas, M. G., Palmucci, M., & Tagliazucchi, E. (2018). Dynamic
858 functional connectivity and brain metastability during altered states of consciousness.
859 *NeuroImage*, 180, 383–395. <https://doi.org/10.1016/j.neuroimage.2017.09.065>
- 860 Chennu, S., O'Connor, S., Adapa, R., Menon, D. K., & Bekinschtein, T. A. (2016).
861 Brain Connectivity Dissociates Responsiveness from Drug Exposure during Propofol-
862 Induced Transitions of Consciousness. *PLoS Computational Biology*, 12(1),
863 e1004669. <https://doi.org/10.1371/journal.pcbi.1004669>
- 864 Coppola, P., Allanson, J., Naci, L., Adapa, R., Finoia, P., Williams, G. B., Pickard, J.
865 D., Owen, A. M., Menon, D. K., & Stamatakis, E. A. (2022). The complexity of the
866 stream of consciousness. *Communications Biology*, 5(1), 1173.
867 <https://doi.org/10.1038/s42003-022-04109-x>
- 868 Davison, A., & Hinkley, D. (1997). Bootstrap Methods and Their Application. *Journal
869 of the American Statistical Association*, 94. <https://doi.org/10.2307/1271471>
- 870 Deeley, Q., Walsh, E., Oakley, D. A., Bell, V., Koppel, C., Mehta, M. A., & Halligan,
871 P. W. (2013). Using Hypnotic Suggestion to Model Loss of Control and Awareness of
872 Movements: An Exploratory fMRI Study. *PLoS ONE*, 8(10), e78324.
873 <https://doi.org/10.1371/journal.pone.0078324>
- 874 Dor-Ziderman, Y., Ataria, Y., Fulder, S., Goldstein, A., & Berkovich-Ohana, A. (2016).
875 Self-specific processing in the meditating brain: A MEG neurophenomenology study.
876 *Neuroscience of Consciousness*, 2016(1), niw019. <https://doi.org/10.1093/nc/niw019>
- 877 Ermentrout, G. B., & Cowan, J. D. (1979). A mathematical theory of visual
878 hallucination patterns. *Biological Cybernetics*, 34(3), 137–150.
879 <https://doi.org/10.1007/BF00336965>

- 880 Fort, L. D., Costines, C., Wittmann, M., Demertzi, A., & Schmidt, T. T. (2025).
881 Classification schemes of altered states of consciousness. *Neuroscience &*
882 *Biobehavioral Reviews*, 175, 106178.
883 <https://doi.org/10.1016/j.neubiorev.2025.106178>
- 884 Ganesan, S., Yang, W. F. Z., Chowdhury, A., Zalesky, A., & Sacchet, M. D. (2024).
885 Within-subject reliability of brain networks during advanced meditation: An intensively
886 sampled 7 Tesla MRI case study. *Human Brain Mapping*, 45(7), e26666.
887 <https://doi.org/10.1002/hbm.26666>
- 888 Gattuso, J. J., Perkins, D., Ruffell, S., Lawrence, A. J., Hoyer, D., Jacobson, L. H.,
889 Timmermann, C., Castle, D., Rossell, S. L., Downey, L. A., Pagni, B. A., Galvão-
890 Coelho, N. L., Nutt, D., & Sarris, J. (2023). Default Mode Network Modulation by
891 Psychedelics: A Systematic Review. *International Journal of
892 Neuropsychopharmacology*, 26(3), 155–188. <https://doi.org/10.1093/ijnp/pyac074>
- 893 Gosseries, O., Marie, N., Lafon, Y., Bicego, A., Grégoire, C., Oswald, V., &
894 Vanhaudenhuyse, A. (2024). Exploration of trance states: Phenomenology, brain
895 correlates, and clinical applications. *Current Opinion in Behavioral Sciences*, 58,
896 101400. <https://doi.org/10.1016/j.cobeha.2024.101400>
- 897 Grégoire, C., Sombrun, C., Lenaif, P., Marie, N., Giovine, A., Walter, M., Gosseries,
898 O., & Vanhaudenhuyse, A. (2024). Phenomenological characteristics of auto-induced
899 cognitive trance and Mahorikatan® trance. *Neuroscience of Consciousness*, 2024(1),
900 niae024. <https://doi.org/10.1093/nc/niae024>
- 901 Hasenkamp, W., Wilson-Mendenhall, C. D., Duncan, E., & Barsalou, L. W. (2012).
902 Mind wandering and attention during focused meditation: A fine-grained temporal
903 analysis of fluctuating cognitive states. *NeuroImage*, 59(1), 750–760.
904 <https://doi.org/10.1016/j.neuroimage.2011.07.008>
- 905 Hove, M. J., Stelzer, J., Nierhaus, T., Thiel, S. D., Gundlach, C., Margulies, D. S.,
906 Van Dijk, K. R. A., Turner, R., Keller, P. E., & Merker, B. (2016). Brain Network
907 Reconfiguration and Perceptual Decoupling During an Absorptive State of

- 908 Consciousness. *Cerebral Cortex*, 26(7), 3116–3124.
909 <https://doi.org/10.1093/cercor/bhv137>
- 910 Huels, E. R., Kim, H., Lee, U., Bel-Bahar, T., Colmenero, A. V., Nelson, A., Blain-
911 Moraes, S., Mashour, G. A., & Harris, R. E. (2021). Neural Correlates of the
912 Shamanic State of Consciousness. *Frontiers in Human Neuroscience*, 15, 610466.
913 <https://doi.org/10.3389/fnhum.2021.610466>
- 914 Kamada, T., & Kawai, S. (1989). AN ALGORITHM FOR DRAWING GENERAL
915 UNDIRECTED GRAPHS. *INFORMATION PROCESSING LETTERS*, 31(1).
- 916 Kay, S. R., Fiszbein, A., & Opler, L. A. (1987). The Positive and Negative Syndrome
917 Scale (PANSS) for Schizophrenia. *Schizophrenia Bulletin*, 13(2), 261–276.
918 <https://doi.org/10.1093/schbul/13.2.261>
- 919 Lanfranco, R. C., Rivera-Rei, Á., Huepe, D., Ibáñez, A., & Canales-Johnson, A.
920 (2021). Beyond imagination: Hypnotic visual hallucination induces greater lateralised
921 brain activity than visual mental imagery. *NeuroImage*, 239, 118282.
922 <https://doi.org/10.1016/j.neuroimage.2021.118282>
- 923 Lewis-Healey, E., Tagliazucchi, E., Canales-Johnson, A., & Bekinschtein, T. A.
924 (2024). Breathwork-induced psychedelic experiences modulate neural dynamics.
925 *Cerebral Cortex*, 34(8), bhae347.
- 926 Mainieri, A. G., Peres, J. F. P., Moreira-Almeida, A., Mathiak, K., Habel, U., & Kohn,
927 N. (2017). Neural correlates of psychotic-like experiences during spiritual-trance
928 state. *Psychiatry Research: Neuroimaging*, 266, 101–107.
929 <https://doi.org/10.1016/j.pscychresns.2017.06.006>
- 930 Mateos, D. M., Guevara Erra, R., Wennberg, R., & Perez Velazquez, J. L. (2018).
931 Measures of entropy and complexity in altered states of consciousness. *Cognitive
932 Neurodynamics*, 12(1), 73–84. <https://doi.org/10.1007/s11571-017-9459-8>
- 933 Mindlin, I., Herzog, R., Belloli, L., Manasova, D., Monge-Asensio, M., Vohryzek, J.,
934 Escrichs, A., Alnagger, N., Núñez, P., Gosseries, O., Kringlebach, M. L., Deco, G.,
935 Tagliazucchi, E., Naccache, L., Rohaut, B., Sitt, J. D., & Sanz Perl, Y. (2024). Whole

- 936 brain modelling for simulating pharmacological interventions on patients with
937 disorders of consciousness. *Communications Biology*, 7(1), 1–13.
938 <https://doi.org/10.1038/s42003-024-06852-9>
- 939 Miyashita, Y. (1995). How the Brain Creates Imagery: Projection to Primary Visual
940 Cortex. *Science*, 268(5218), 1719–1720. <https://doi.org/10.1126/science.7792596>
- 941 Oswald, V., Jerbi, K., Sombrun, C., Jitka, A., Martial, C., Gosseries, O., &
942 Vanhaudenhuyse, A. (2025). Understanding individual differences in non-ordinary
943 state of consciousness: Relationship between phenomenological experiences and
944 autonomic nervous system. *International Journal of Clinical and Health Psychology :
IJCCHP*, 25(1), 100552. <https://doi.org/10.1016/j.ijchp.2025.100552>
- 945 Pessa, A. A. B., & Ribeiro, H. V. (2021). ordpy: A Python package for data analysis
946 with permutation entropy and ordinal network methods. *Chaos: An Interdisciplinary
947 Journal of Nonlinear Science*, 31(6), 063110. <https://doi.org/10.1063/5.0049901>
- 948 Petitmengin, C. (2006). Describing One's Subjective Experience in the Second
949 Person: An Interview Method for the Science of Consciousness. *Phenomenology
950 and the Cognitive Sciences*, 5(3–4), 229–269. [https://doi.org/10.1007/s11097-006-9022-2](https://doi.org/10.1007/s11097-006-
951 9022-2)
- 952 Quigley, K. S., Kanoski, S., Grill, W. M., Barrett, L. F., & Tsakiris, M. (2021).
953 Functions of Interoception: From Energy Regulation to Experience of the Self.
954 *Trends in Neurosciences*, 44(1), 29–38. <https://doi.org/10.1016/j.tins.2020.09.008>
- 955 Rogerson, R. G., Barnstaple, R. E., & DeSouza, J. F. (2021). Neural Correlates of a
956 Trance Process and Alternative States of Consciousness in a Traditional Healer.
957 *Brain Sciences*, 11(4), 497. <https://doi.org/10.3390/brainsci11040497>
- 958 Roseman, L., Demetriou, L., Wall, M. B., Nutt, D. J., & Carhart-Harris, R. L. (2018).
959 Increased amygdala responses to emotional faces after psilocybin for treatment-
960 resistant depression. *Neuropharmacology*, 142, 263–269.
961 <https://doi.org/10.1016/j.neuropharm.2017.12.041>

- 963 Salomon, R., Ronchi, R., Dönz, J., Bello-Ruiz, J., Herbelin, B., Martet, R., Faivre, N.,
964 Schaller, K., & Blanke, O. (2016). The Insula Mediates Access to Awareness of
965 Visual Stimuli Presented Synchronously to the Heartbeat. *The Journal of
966 Neuroscience: The Official Journal of the Society for Neuroscience*, 36(18), 5115–
967 5127. <https://doi.org/10.1523/JNEUROSCI.4262-15.2016>
- 968 Seitzman, B. A., Gratton, C., Marek, S., Raut, R. V., Dosenbach, N. U. F., Schlaggar,
969 B. L., Petersen, S. E., & Greene, D. J. (2020). A set of functionally-defined brain
970 regions with improved representation of the subcortex and cerebellum. *NeuroImage*,
971 206, 116290. <https://doi.org/10.1016/j.neuroimage.2019.116290>
- 972 Siegel, R. K. (1977). Hallucinations. *Scientific American*, 237(4), 132–140.
973 <https://doi.org/10.1038/scientificamerican1077-132>
- 974 Siegel, R. K., & Jarvik, M. E. (1975). Drug-induced hallucinations in animals and
975 man. *Hallucinations: Behavior, Experience and Theory*, 81, 161.
- 976 Smigielski, L., Scheidegger, M., Komter, M., & Vollenweider, F. X. (2019).
977 Psilocybin-assisted mindfulness training modulates self-consciousness and brain
978 default mode network connectivity with lasting effects. *NeuroImage*, 196, 207–215.
979 <https://doi.org/10.1016/j.neuroimage.2019.04.009>
- 980 Stamatakis, E. A., Adapa, R. M., Absalom, A. R., & Menon, D. K. (2010). Changes in
981 Resting Neural Connectivity during Propofol Sedation. *PLOS ONE*, 5(12), e14224.
982 <https://doi.org/10.1371/journal.pone.0014224>
- 983 Stawarczyk, D., Majerus, S., Maj, M., Van der Linden, M., & D'Argembeau, A. (2011).
984 Mind-wandering: Phenomenology and function as assessed with a novel experience
985 sampling method. *Acta Psychologica*, 136(3), 370–381.
986 <https://doi.org/10.1016/j.actpsy.2011.01.002>
- 987 Stoliker, D., Novelli, L., Vollenweider, F. X., Egan, G. F., Preller, K. H., & Razi, A.
988 (2024). Neural Mechanisms of Resting-State Networks and the Amygdala Underlying
989 the Cognitive and Emotional Effects of Psilocybin. *Biological Psychiatry*.
990 <https://doi.org/10.1016/j.biopsych.2024.01.002>

- 991 Tagliazucchi, E., Roseman, L., Kaelen, M., Orban, C., Muthukumaraswamy, S. D.,
992 Murphy, K., Laufs, H., Leech, R., McGonigle, J., Crossley, N., Bullmore, E., Williams,
993 T., Bolstridge, M., Feilding, A., Nutt, D. J., & Carhart-Harris, R. (2016). Increased
994 Global Functional Connectivity Correlates with LSD-Induced Ego Dissolution.
995 *Current Biology*, 26(8), 1043–1050. <https://doi.org/10.1016/j.cub.2016.02.010>
- 996 Tagliazucchi, E., & van Someren, E. J. W. (2017). The large-scale functional
997 connectivity correlates of consciousness and arousal during the healthy and
998 pathological human sleep cycle. *NeuroImage*, 160, 55–72.
999 <https://doi.org/10.1016/j.neuroimage.2017.06.026>
- 1000 Tart, C. (1976). _.'The Basic Nature of Altered States of Consciousness, A System
1001 Approach'. *Journal of Transpersonal Psychology*, 1.
1002 <https://www.atpweb.org/jtparchive/trps-08-76-01-045.pdf>
- 1003 Timmermann, C., Bauer, P. R., Gosseries, O., Vanhaudenhuyse, A., Vollenweider,
1004 F., Laureys, S., Singer, T., Antonova, E., & Lutz, A. (2023). A
1005 neurophenomenological approach to non-ordinary states of consciousness:
1006 Hypnosis, meditation, and psychedelics. *Trends in Cognitive Sciences*, 27(2), 139–
1007 159. <https://doi.org/10.1016/j.tics.2022.11.006>
- 1008 Timmermann, C., Watts, R., & Dupuis, D. (2022). Towards psychedelic
1009 apprenticeship: Developing a gentle touch for the mediation and validation of
1010 psychedelic-induced insights and revelations. *Transcultural Psychiatry*.
1011 <https://doi.org/10.1177/13634615221082796>
- 1012 Tsakiris, M., & Critchley, H. (2016). Interoception beyond homeostasis: Affect,
1013 cognition and mental health. *Philosophical Transactions of the Royal Society B:
1014 Biological Sciences*, 371(1708), 20160002. <https://doi.org/10.1098/rstb.2016.0002>
- 1015 Vanhaudenhuyse, A., Castillo, M.-C., Martial, C., Annen, J., Bicego, A., Rousseaux,
1016 F., Sanz, L. R. D., Sombrun, C., Bioy, A., & Gosseries, O. (2024). Phenomenology of
1017 auto-induced cognitive trance using text mining: A prospective and exploratory group

1018 study. *Neuroscience of Consciousness*, 2024(1), niae036.
1019 <https://doi.org/10.1093/nc/niae036>
1020 Whitfield-Gabrieli, S., & Nieto-Castanon, A. (2012). *Conn: A Functional Connectivity*
1021 *Toolbox for Correlated and Anticorrelated Brain Networks*. *Brain Connectivity*, 2(3),
1022 125–141. <https://doi.org/10.1089/brain.2012.0073>
1023 Yang, W. F. Z., Chowdhury, A., Bianciardi, M., van Luttermeld, R., Sparby, T., &
1024 Sacchet, M. D. (2023). Intensive whole-brain 7T MRI case study of volitional control
1025 of brain activity in deep absorptive meditation states. *Cerebral Cortex (New York,*
1026 *NY)*, 34(1), bhad408. <https://doi.org/10.1093/cercor/bhad408>

1027

1028 **8. Figure legends**

1029 **Figure 1. Analysis pipeline.** a) Experimental design: The participants underwent MRI
1030 sessions consisting of four functional blocks and one structural block (placed between the
1031 NOC condition and the Residual condition to allow the participants to return to the Baseline).
1032 b) We parceled the brain into 288 regions of interest, from which we constructed correlation
1033 matrices based on ROIs or functional networks. All studied metrics were calculated from
1034 these matrices. c) We computed the functional connectivity at the network level and the ROI
1035 level, as well using a seed analysis. Within the ROI level, we distinguished between intra-
1036 network connectivity (connectivity among ROIs of the same network) and inter-network
1037 connectivity (connectivity among ROIs of different networks). d) We used intra-network and
1038 inter-network functional connectivity to study topographical changes in our participant and
1039 the control group using linear mixed models and force-directed graph projections.

1040

1041 **Figure 2. Global connectivity changes.** a) Example matrices of how we calculated intra-
1042 network functional connectivity (left) and inter-network connectivity (right). Intra-network
1043 functional connectivity is defined as the average correlation values between ROIs of the
1044 same functional network. Inter-network connectivity is defined as the average correlation
1045 values between ROIs i and j such that i belongs to one functional network and j belongs to
1046 another functional network. b) Intra-network connectivity for each experimental condition.
1047 Individual points represent AVP's sessions, and the bars denote the standard error of the
1048 mean (S.E.M.). An asterisk indicates $p < 0.05$, and two asterisks indicate $p < 0.01$, both FDR
1049 corrected. NOC and Residual conditions are significantly different from Baseline. c) Inter-
1050 network connectivity for each experimental condition. Individual points represent AVP's

1051 sessions, and the bars denote the S.E.M. All conditions differ significantly from Baseline. d)
1052 Intra- and inter-network connectivity normalized to Baseline. Intra-network connectivity
1053 remains almost unchanged across conditions, while inter-network connectivity decreases
1054 significantly, suggesting a dissolution of inter-network relationships and maintenance of
1055 functional networks. e-g) Two-dimensional maps showing changes in intra-network
1056 connectivity (x-axis) and inter-network connectivity (y-axis). The base of the arrow
1057 represents the intra- and inter-network pair characterizing the Baseline, while the arrow's
1058 endpoint marks the value in each experimental condition. Thus, the arrow's magnitude
1059 indicates the change between the specified condition and Baseline. Asterisks indicate $p <$
1060 0.05. The nodes corresponding to functional networks whose connectivity changes across
1061 conditions were statistically significant were colored using the FN's specific color. h)
1062 Standard deviation (top) and Coefficient of Variation (bottom), as a proxy for absolute and
1063 relative functional connectivity variability.

1064

1065 **Figure 3. Permutation entropy and Statistical complexity.** a) The entropy shows
1066 significant differences between Baseline and Transition, and Baseline and NOC, but no
1067 difference between Baseline and Residual. b) The complexity shows a similar behavior with
1068 differences between Baseline and Transition, and Baseline and NOC but no difference
1069 between Baseline and Residual. A triple asterisk indicates $p < 0.001$. c) Entropy-Complexity
1070 plane. Initially, Baseline starts with high entropy and low complexity. As it progresses to
1071 Transition and NOC, the entropy decreases and complexity increases. Finally, the condition
1072 Residual returns to similar levels of entropy and complexity as Baseline. The bars denote
1073 standard error of the mean.

1074

1075 **Figure 4. Network-level connectivity changes.** Difference in inter-network connectivity for
1076 each condition compared to baseline. Asterisks indicate significance in the linear mixed
1077 model (FDR corrected); see Table S3 for a complete list of significant network pairs. Blue
1078 lines signify a decrease relative to baseline, while red lines indicate an increase. DA =
1079 Dorsal Attention; MTL = Medial Temporal Lobe; DMN = Default Mode Network; Rew =
1080 Reward; SN = Salience Network; FP = Frontoparietal; SMD = Somatomotor Dorsal; SML =
1081 Somatomotor Lateral; VA = Ventral Attention; CO = Cingulo-Opercular; VIS = Visual; AUD =
1082 Auditive; PM = Parieto-medial.

1083

1084 **Figure 5. ROI-based connectivity.** a) Topology of AVP connectivity: minimal energy plots
1085 of the average networks for all conditions. It is notable how the visual network becomes
1086 isolated from the rest in the NOC and Residual conditions compared to Baseline. b) Glass
1087 brain visualizations showing regions of interest (ROIs) with significant changes in

1088 connectivity for each experimental condition relative to baseline after correction. Each panel
1089 corresponds to one comparison: Transition vs. Baseline, NOC vs. Baseline, and Residual vs.
1090 Baseline. ROIs displayed in the upper half of each brain showed increased connectivity
1091 relative to baseline, while those in the lower half showed decreased connectivity. Note that
1092 significance is assessed at the ROI level, independent of network identity; thus, the
1093 prominence of a given color reflects the network associated with that particular ROI. See
1094 Table S5 for the full list of significant network pairs.

1095

1096 **Figure 6. Network-level Seed-Based Connectivity Analysis.** Seed-based functional
1097 connectivity analysis using significant ROIs from Figure 5 within four large-scale networks:
1098 visual (a), dorsal somatomotor (b), frontoparietal (c), and salience (d). For each network,
1099 connectivity maps were computed for each ROI and subsequently averaged to obtain a
1100 network-level correlation map. Statistical significance was assessed using FDR correction at
1101 0.05, and only surviving voxels are displayed.

1102 **Table 1. Neurophenomenological matrix linking subjective experience with brain**
1103 **network dynamics.**

1104 **Supplementary Figure S1. Global connectivity without movement** (a) Intra-network and
1105 (b) inter-network connectivity for each experimental condition after removing 3 scans before
1106 and after the foot movement. Individual points represent AVP's sessions, and the bars
1107 denote the standard error of the mean (S.E.M.). Results replicate those shown in Figure 2b
1108 and 2c, with the same statistical significance. An asterisk indicates $p < 0.05$, and two
1109 asterisks indicate $p < 0.01$, both FDR corrected.

1110 **Supplementary Figure S2. Connectivity Across Conditions in the Control Group.** a)
1111 Global intra-connectivity (left), inter-connectivity (middle) and variation coefficient (right). A
1112 statistically significant difference was observed only in inter-network connectivity between
1113 Baseline and NOC conditions. b) Normalized connectivity increases in the NOC state in
1114 controls, the opposite effect as AVP.

1115 **Supplementary Figure S3. Intra and inter-connectivity map in controls.** a) Two-
1116 dimensional maps showing changes in intra-network connectivity (x-axis) and inter-network
1117 connectivity (y-axis) within controls. The base of the arrow represents the intra- and inter-
1118 network pair characterizing the Baseline, while the arrow's endpoint marks the value in each
1119 experimental condition. Thus, the arrow's magnitude indicates the change between the
1120 specified condition and Baseline. No significant changes were observed between conditions
1121 in the control group.

1122 **Supplementary Figure S4. Network-level connectivity.** a) Changes in functional networks
1123 at the network level for networks that show significant changes in connectivity compared to
1124 Baseline. The visual, sensorimotor dorsal, and ventral attention networks diminish their
1125 connectivity compared to Baseline, while the Frontoparietal and Salience networks increase
1126 their connectivity. b) Network-level connectivity for the control group. No statistically
1127 significant differences were found between conditions.

1128 **Supplementary Figure S5.** Entropy-Complexity distribution for the four experimental
1129 conditions: the Baseline, Transition, NOC and Residual using different embedding
1130 parameters from d=2 to d=4, and tau=1 to tau=3.

1131 **Supplementary Figure S6.** Entropy-Complexity plane for different embedding parameters
1132 ranging from d=2 to d=4 and tau=1 to tau=3.

1133 **Table S1. Demographic data of the control group.**

1134 **Table S2. AVP's reported phenomenological experience for each session.**

1135 **Table S3. List of significant network pairs from Figure 4.**

1136 **Table S4. List of network pairs for the control group**

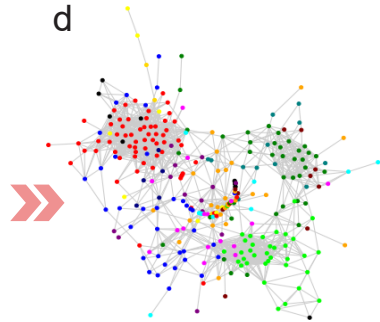
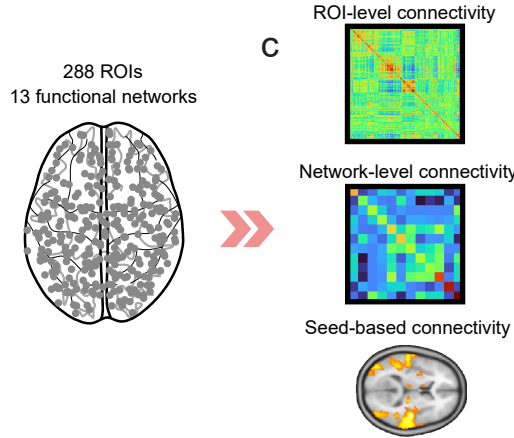
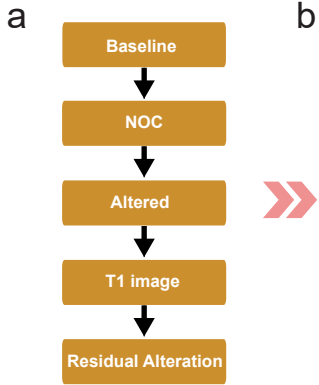
1137 **Table S5. List of significant ROIs in the analysis from Figure 5b.**

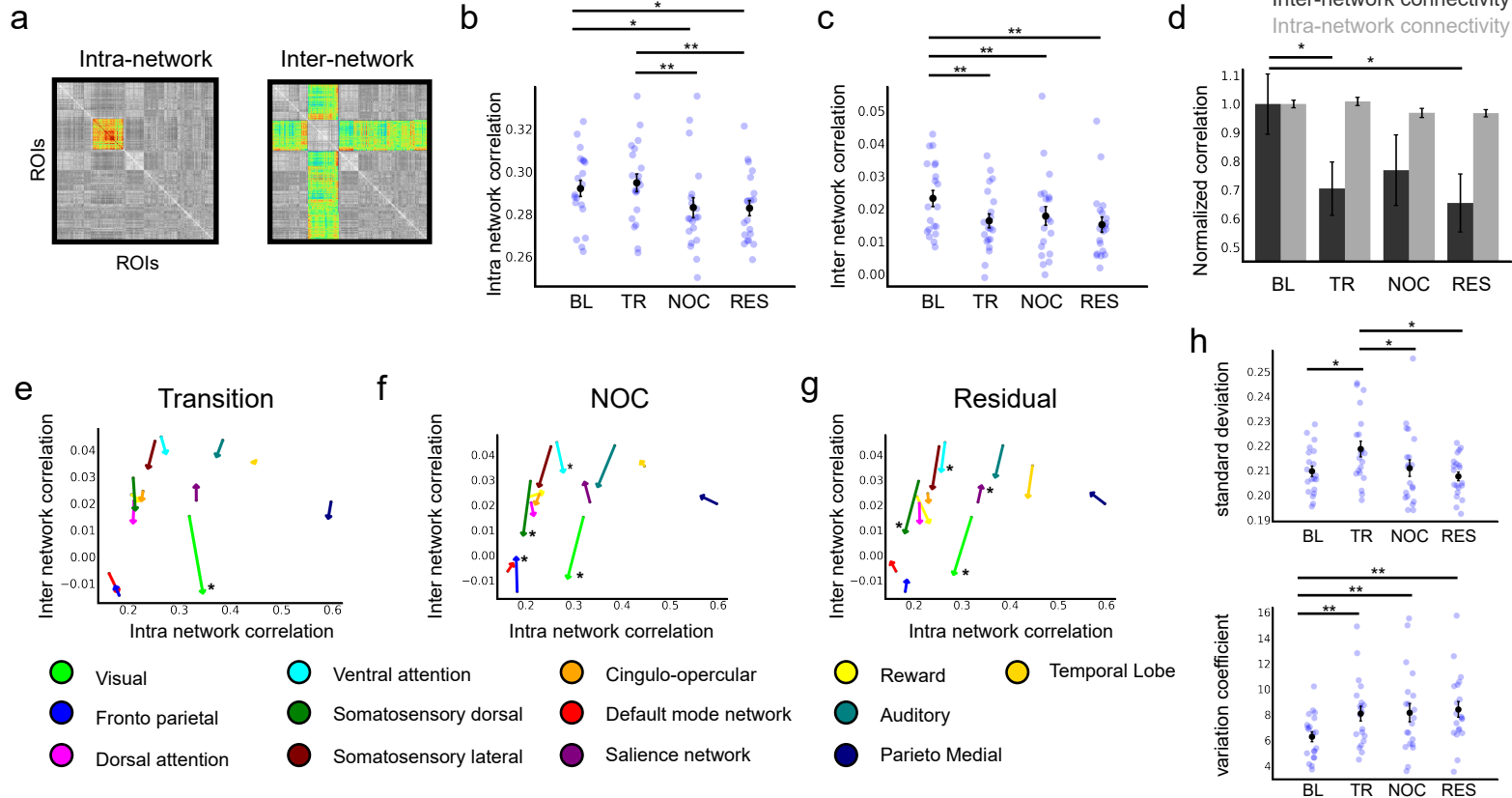
1138 **Table S6. Report of significant clusters for the seed analysis of visual network.**

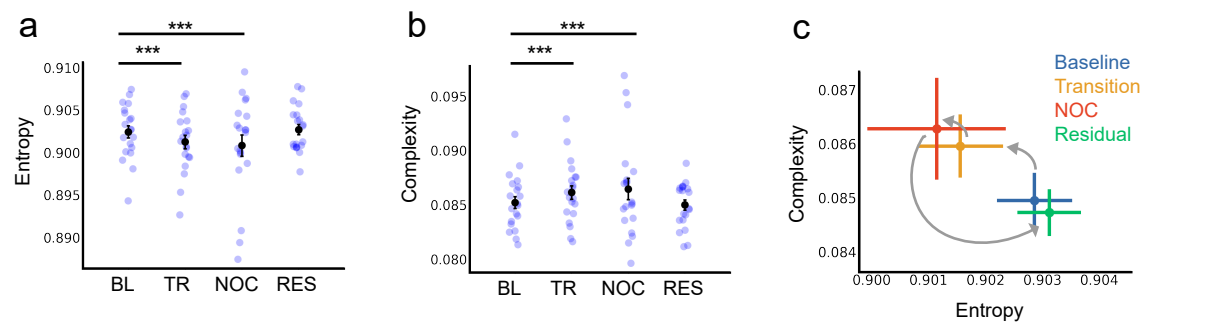
1139 **Table S7. Report of significant clusters for the seed analysis of sensorimotor dorsal
1140 network.**

1141 **Table S8. Report of significant clusters for the seed analysis of fronto-parietal
1142 network.**

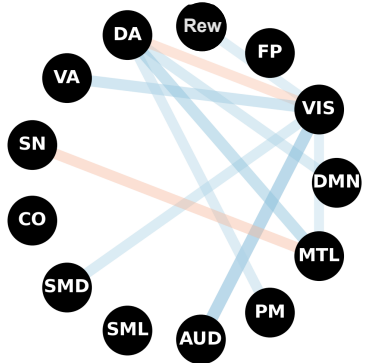
1143 **Table S9. Report of significant clusters for the seed analysis of salience network.**



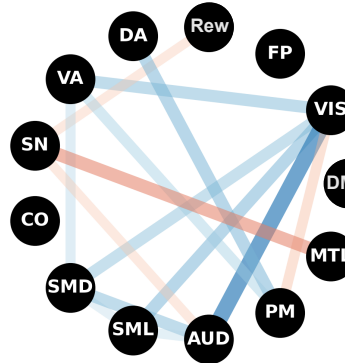




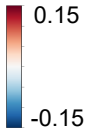
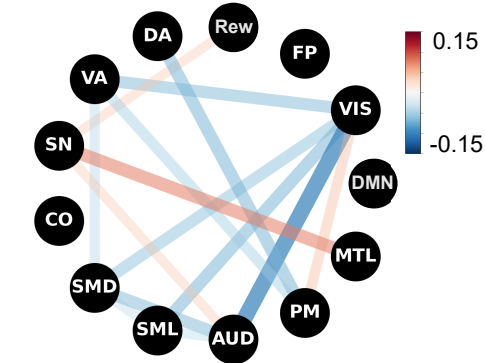
Transition v. Baseline

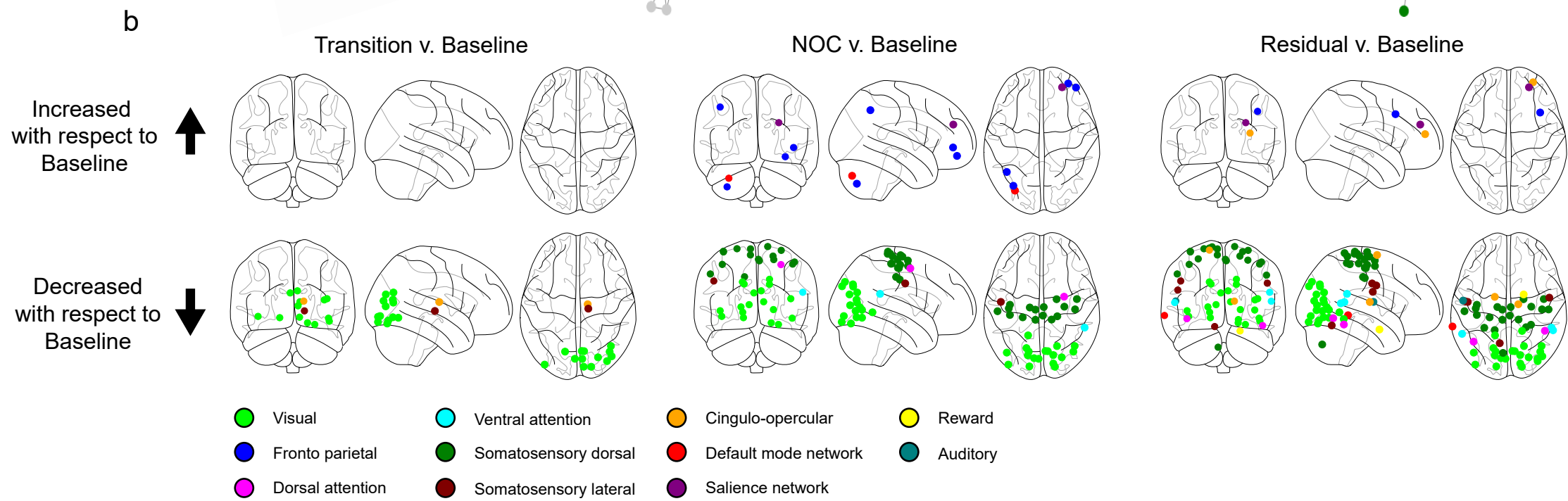
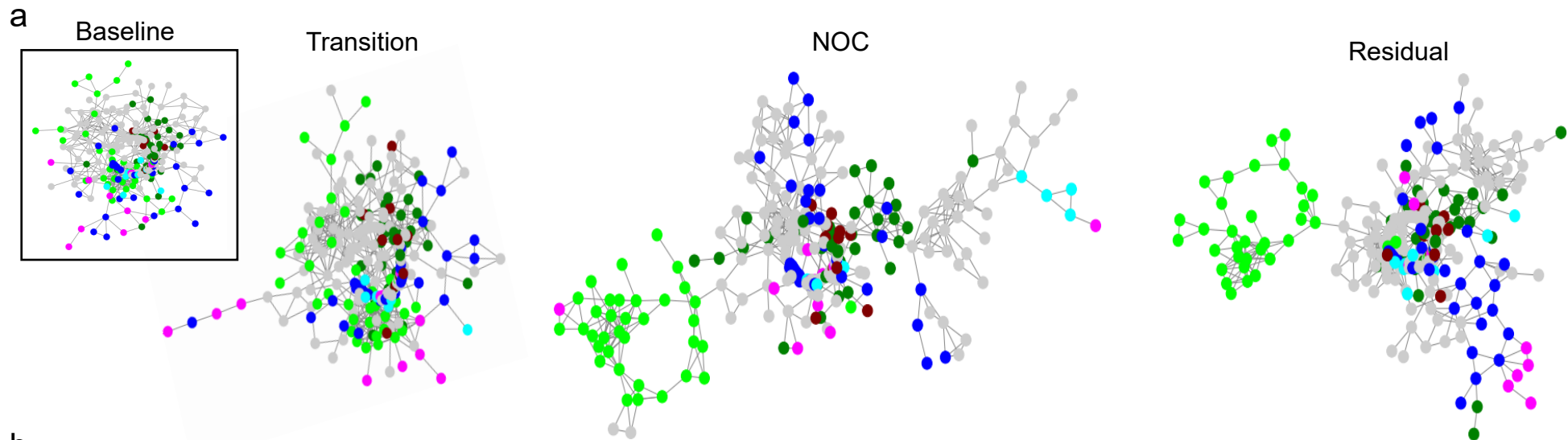


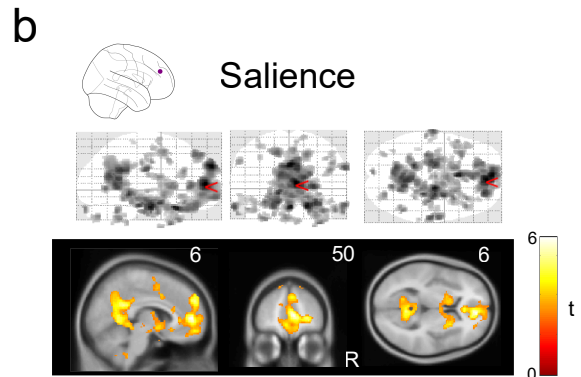
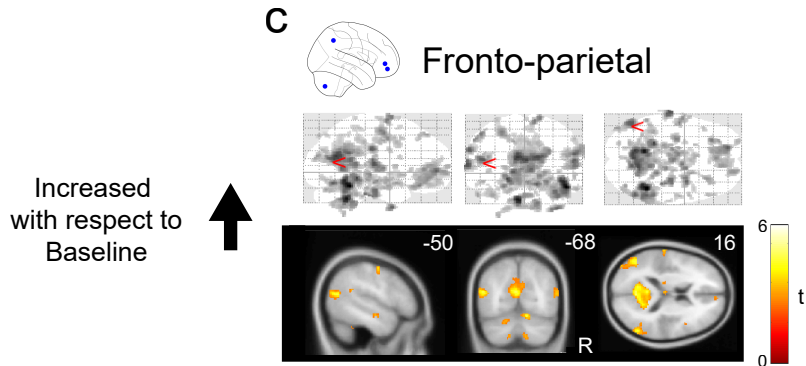
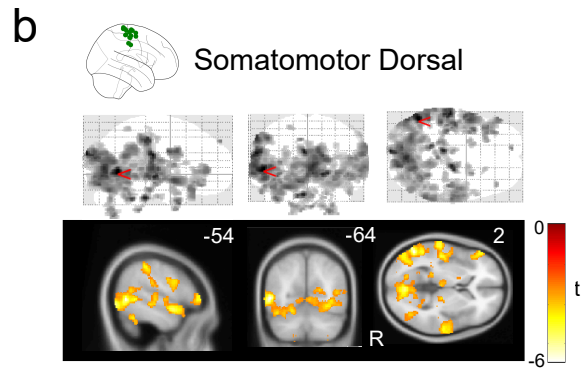
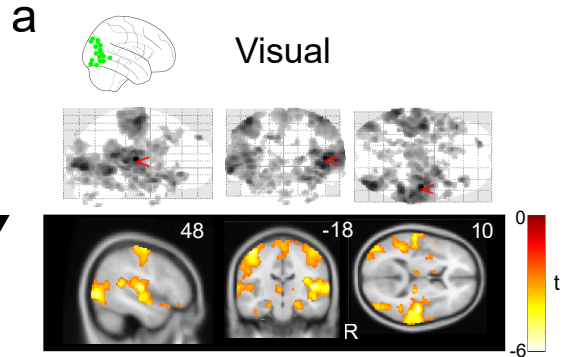
NOC v. Baseline

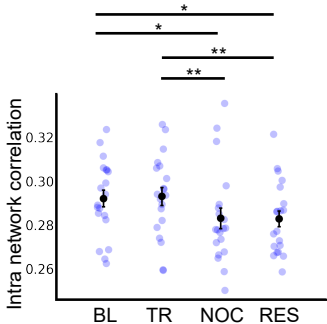
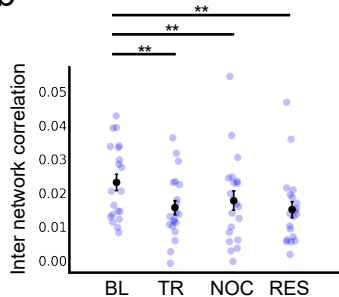


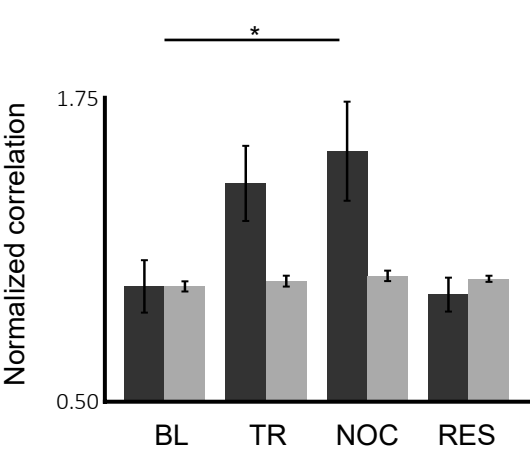
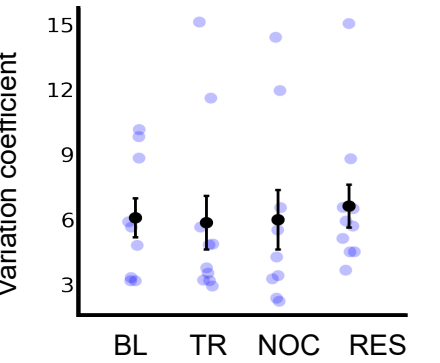
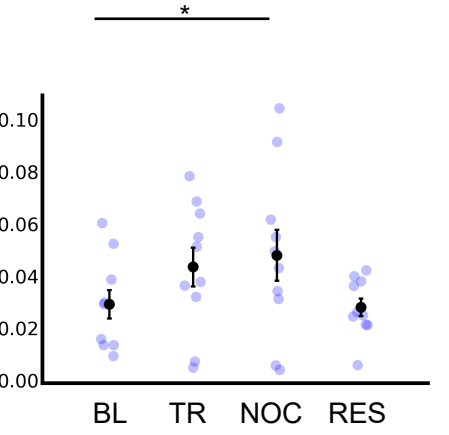
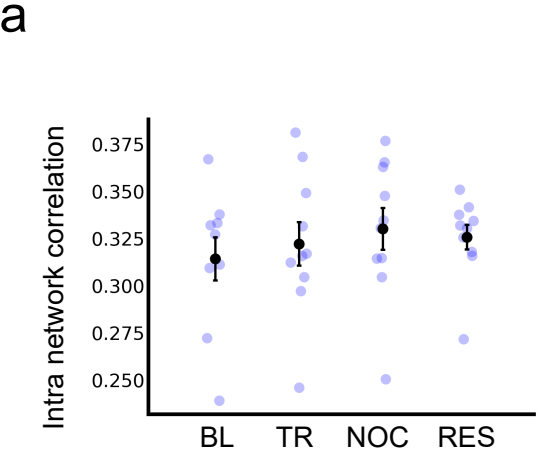
Residual v. Baseline



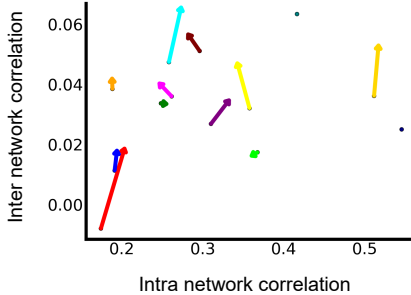




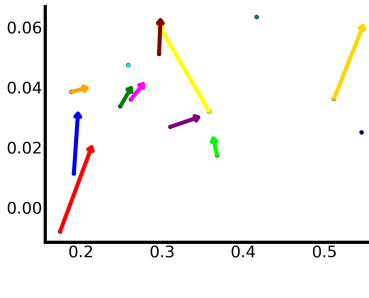
a**b**



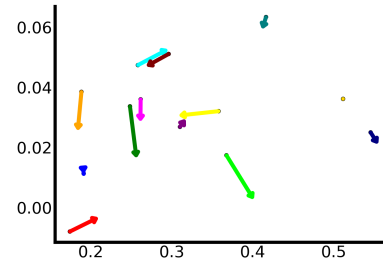
Transition

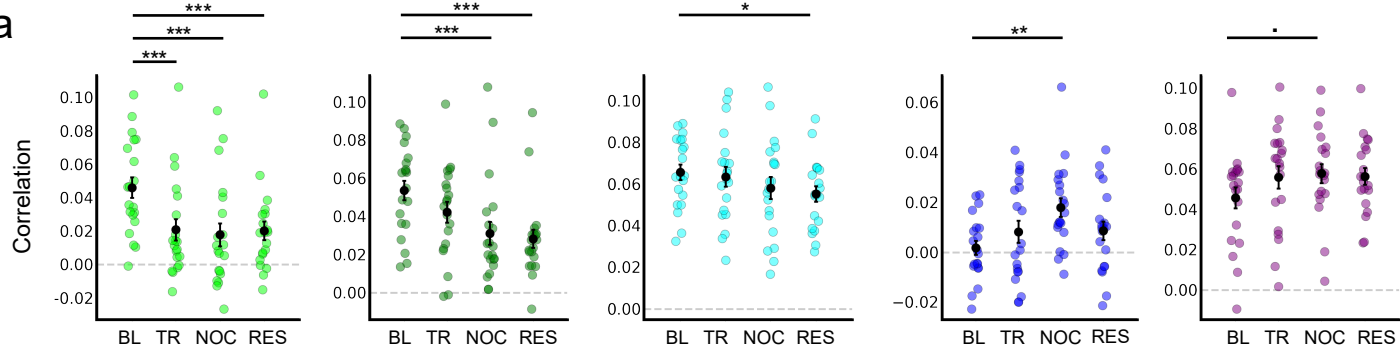
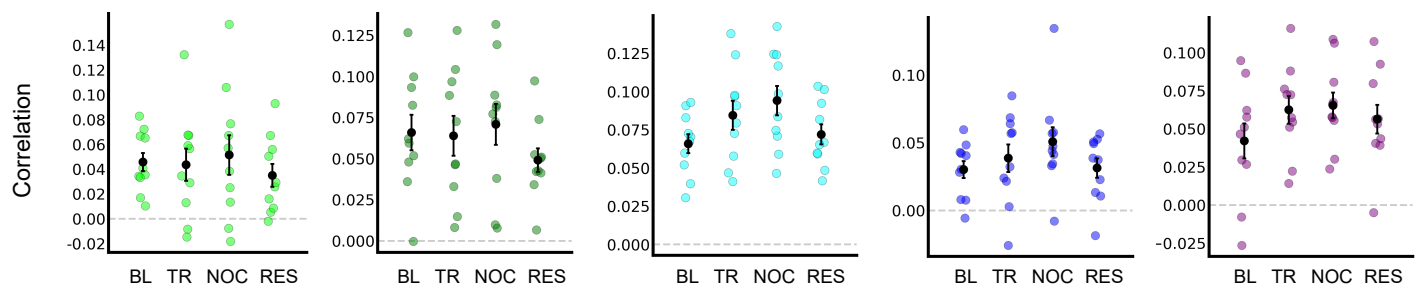


NOC



Residual



a**b**

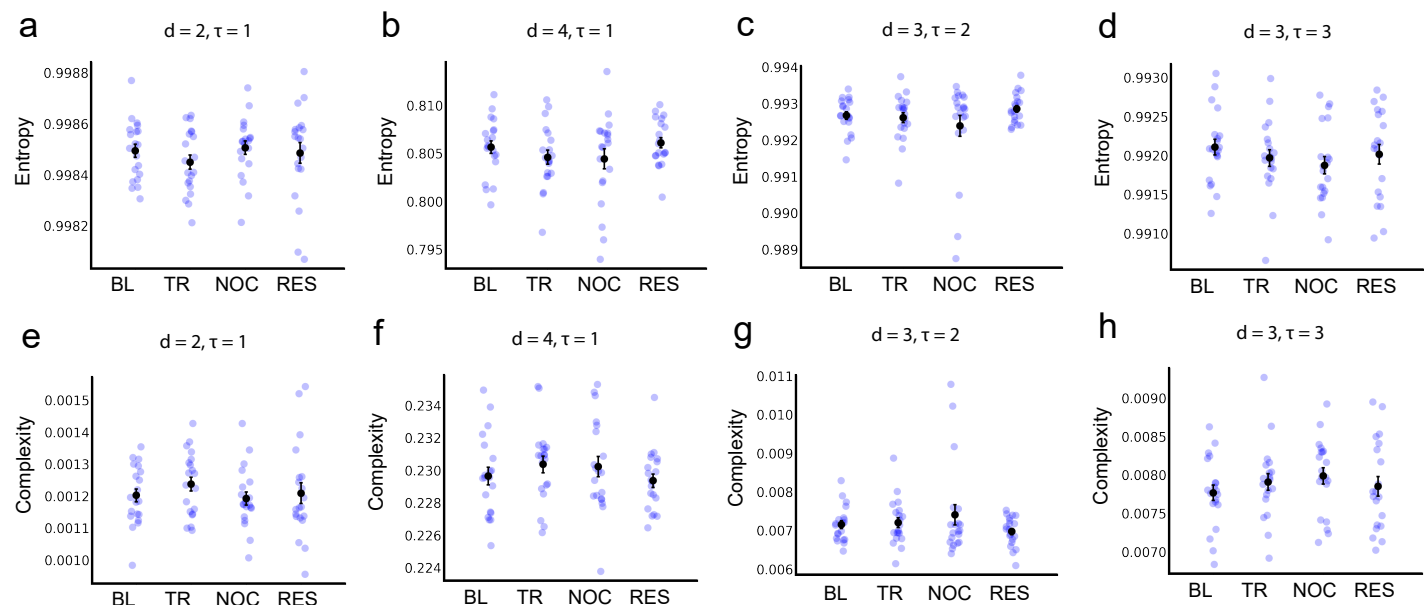
Visual

Somatosensory dorsal

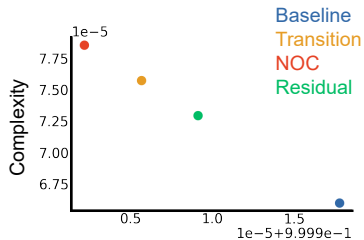
Ventral Attention

Fronto Parietal

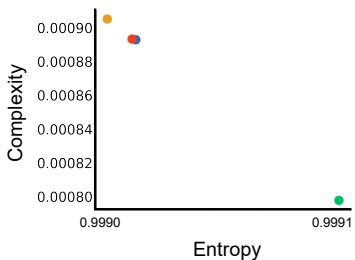
Salience



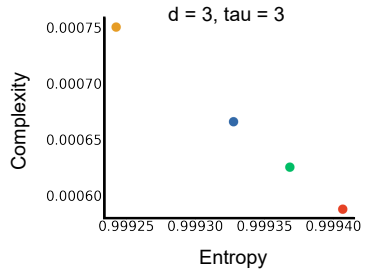
a $d = 2, \tau = 1$



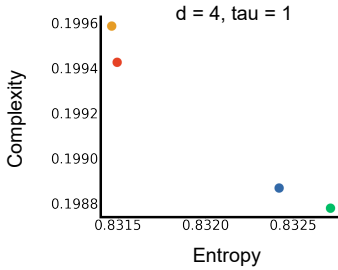
b $d = 3, \tau = 2$



c $d = 3, \tau = 3$



d $d = 4, \tau = 1$



Condition	Subjective experience	Neuroimaging findings
Baseline	<ul style="list-style-type: none"> • Ordinary mentation. • Full bodily awareness. Stable proprioception. • Intentional relaxation and body scanning. • Scanner sound perceived as steady, neutral background. 	<ul style="list-style-type: none"> • Baseline-range intra/inter-network connectivity. • Low global variability. • High entropy, low complexity.
Transition	<ul style="list-style-type: none"> • Effortful and unstable shift. Bodily tension. • Hexagonal, honeycomb imagery, dynamic brightness. • After threshold, “Double-consciousness”: scanner awareness + emerging unity. • Sense of expansion; altered time. 	<ul style="list-style-type: none"> • Peak global variability (high STD, high CV). • Early inter-network decoupling (VIS→VA/AUD/SMD). • ROI-level decreases (visual, CO, SMD). • Entropy diminishes, complexity increases.
NOC	<ul style="list-style-type: none"> • Stable immersive visionary mode. • Vivid geometric imagery: violet grids, fractals, pulses. • Altered embodiment. Proprioceptive attenuation. • Scanner sound treated as mantra. • Serenity, unity, timelessness. Deep stable absorption. 	<ul style="list-style-type: none"> • Strong inter-network decoupling (VIS, SMD, VA). • VIS isolated. • VIS: broad decoupling from auditory, somatomotor, pulvinar, cerebellum. • SMD: decoupling from auditory/language regions. • FP: increased connectivity with PCC/precuneus, mPFC, SMA, temporal multimodal,

cerebellum.

- SN: increased connectivity with PCC/precuneus, insula, thalamus, early visual.
- Entropy lower, complexity highest.

Residual

- Abrupt disruption then slow return.
- Persisting perceptual alterations (brightness, soft borders).
- Gradual re-entry into ordinary mentation.
- Partial reconnection but still low inter-network connectivity vs Baseline.
- VIS/SMD remain partially decoupled.
- SN mildly more connected.
- Entropy/complexity return to baseline.